A Pictorial Account of Heart Development: Spatial and Temporal Aspects of The Human Embryonic Heart Between 3.5 and 8 Weeks of Development

Jill Hikspoors (jill.hikspoors@maastrichtuniversity.nl)
Maastricht University https://orcid.org/0000-0003-2940-1812
Nuthmethee Kruepunga
Maastricht University
Greet Mommen
Maastricht University
Eleonore Koehler
Maastricht University
Robert Anderson
Newcastle University https://orcid.org/0000-0001-5163-9021
Wouter Lamers
Maastricht University

Article

Keywords:

Posted Date: December 28th, 2020

DOI: https://doi.org/10.21203/rs.3.rs-129074/v1

Version of Record: A version of this preprint was published at Communications Biology on March 11th, 2022. See the published version at https://doi.org/10.1038/s42003-022-03153-x.

A pictorial account of heart development: spatial and temporal aspects of the human embryonic heart between 3.5 and 8 weeks of development

Jill P.J.M. Hikspoors[1,*], Nutmethee Kruepunga[1,#], Greet M.C. Mommen[1], S. Eleonore Köhler[1], Robert H. Anderson[2], and Wouter H. Lamers[1,3]

[1]Department of Anatomy & Embryology, Maastricht University, Maastricht, The Netherlands; [2]Biosciences Institute, Newcastle University, Newcastle upon Tyne, United Kingdom; [3]Tytgat Institute for Liver and Intestinal Research, Academic Medical Center, Amsterdam, The Netherlands

#: present address: Department of Anatomy, Faculty of Science, Mahidol University, Bangkok, Thailand

* correspondence

Jill P.J.M. Hikspoors, Ph.D. Department of Anatomy & Embryology, Maastricht University, Universiteitssingel 50, 6229 ER Maastricht, The Netherlands. T: +31433881061 E: jill.hikspoors@maastrichtuniversity.nl

Abstract

Heart development is topographically complex and requires visualization to understand its progression. No comprehensive 3-dimensional primer of human cardiac development is currently available. We prepared detailed reconstructions of 12 hearts between 3.5 and 8 weeks post fertilization, using Amira® 3D-reconstruction and Cinema4D®-remodeling software. The models were visualized as calibrated interactive 3D-PDFs. We describe the developmental appearance and subsequent remodeling of 70 different structures incrementally, using sequential segmental analysis. Pictorial timelines of structures highlight age-dependent events, while graphs visualize growth and spiraling of the wall of the heart tube. The basic cardiac layout is established between 3.5 and 4.5 weeks. Septation at the venous pole is completed at 6 weeks. Between 5.5 and 6.5 weeks, as the outflow tract becomes incorporated in the ventricles, the spiraling course of its subaortic and subpulmonary channels is transferred to the intrapericardial arterial trunks. The remodeling of the interventricular foramen is complete at 7 weeks.

Introduction

Embryology is a visual discipline. Many aspects of embryonic development are topographically complex, such that 3-dimensional (3D) models are exceedingly helpful in fully understanding the temporal events. Examples of often used or cited classical models are Born's "Plattenmodellen", and Ziegler's freehand models of embryos, which were studied and described by His [1,2]. Other examples are Blechschmidt's models and drawings of human embryos [3,4], and van Mierop's images of the developing heart [5], which were redrawn by Netter [6]. All these successful approaches have in common that medical artists collaborated with embryologists who had artistic capacities themselves. Because the methods used to make the models were labor-intensive, existing illustrations were often modified rather than new versions being created. An example, documented in detail [7], is the frequently cited treatise of Kramer on the septation of the outflow tract [8]. Such serial modifications, however, tend to propagate concepts rather than observations, and need to be assessed with caution.

The advent of computer-aided reconstruction methods has significantly decreased the time necessary for reconstruction of sectioned bodies. A recent example is the digital atlas of human

development produced by the Amsterdam group [9]. This atlas, however, does not address development of the heart in any detail. Both qualitative [10] and quantitative [11] tabulations are available for development of the human heart. Since nomenclature in the developing heart is notoriously variable, a combination of text and illustrations is necessary to provide an understandable account. In this respect, the description of human cardiac development based on magnetic resonance or fluorescent episcopic microscopy is instructive [12]. The spatial resolution and differential staining properties of these techniques, however, are still limited. To our knowledge, no comprehensive primer of cardiac development is presently available that is based on first-hand segmentation of structures of interest identified in histological sections. Our study has visualized such development in human embryos between 3.5 and 8 weeks of development, extending from Carnegie stages 9 through 23. We describe each of the stages, and the features distinguishing them from the previous stage. The evidence can be inspected in the corresponding interactive 3D-pdfs (Supplemental Figures 2-13).

Results and Discussion

Distinct developmental features in staged human embryonic hearts

Carnegie Stage 9. The heart becomes morphologically identifiable when ~26 days have passed since fertilization [13] and ≥3 somites have formed [14]. The reconstructed specimen is shown in Supplemental Figure 2. This embryo has developed a neural plate that is flanked by 5 somites and somitomeres. The endoderm, shown in gray, is forming the pharynx. It is continuous at its periphery with the yolk sac, shown in darker gray. The horseshoe-shaped pericardial cavity covers the endoderm in front and laterally, where it becomes gradually narrower to end adjacent to the first somite. Gastrulation begins during CS8 (~23 days of development; [15]). By CS9, Hensen's node, which localizes gastrulation, is found at the caudal end of the columns of somitomeres.

The heart is located at the cranial margin of the embryo [7,14]. During CS8, bilateral heart fields, also known as cardiogenic plates, generate cardiac precursors which are morphologically indistinct. The first heart field, which is defined during CS8 [16], and which can be visualized in mice by the expression of transcription factors *Mesp1* [17,18] and *Hcn4* [19], gives rise primarily to the embryonic left ventricle [16,20]. The second heart field becomes defined at the transition from

CS8 to CS9 [16]. It evolves more gradually, and can be visualized by the expression of the transcription factor *Isl1* [21]. The systemic venous sinus does not express the early cardiogenic transcription factor *Nkx2-5*, but does express *Tbx18* [22,23]. Based on molecular data, we infer that the center of the heart develops first, and that the upstream venous and downstream arterial components are added successively.

Supplemental Figure 2, and other reconstructions [9,24] of embryos with ~5 somites, show that the cardiac primordiums, like those in mouse embryos [25], are bilaterally symmetrical. The two tiny vascular networks course in front of the foregut. The vascular channels of the early heart are surrounded by paired, but partially merged swellings of acellular cardiac jelly. They are enclosed within an unpaired but bilaterally symmetrical pericardial cavity, which has a myogenic visceral wall [14]. The distribution of the jelly, which is produced by endoderm and the visceral pericardial wall [26], presages the location of the boundaries of the myocardium, shown by a black line surrounding green stripes in Supplemental Figure 2 (*cf.* [24]). The initially non-luminal endocardial heart tubes gradually canalize, but at first contain only few erythrocytes. At the venous pole, the heart tubes are continuous with an extensive venous plexus on the periphery of the endoderm. At the arterial pole, near the buccopharyngeal membrane, the heart tubes pass the pharynx laterally to join the paired dorsal aortas. In front of the heart, the primordium of the transverse septum forms as a shelf of thick mesoderm between the endoderm and the pericardial cavity (Figure 1).

Carnegie Stage 10. It is within this stage, when ~28 days have passed since fertilization [13], that the heart starts beating [7,27,28]. The reconstructed specimen is shown in Supplemental Figure 3. The neural plate is flanked by 8 somites. It is transforming into a neural tube at the level of somite 4, representing the future junction of the head and neck. The endoderm, shown in gray, is still continuous at its periphery with the yolk sac, which is shown in darker gray.

Within at most 2 days, the heart has transformed into a single endocardial conduit extending between still paired venous and arterial vessels (Figure 2; [14]). The single channel has the embryonic left ventricle as its caudal, and the outflow tract as its cranial, component. The myocardium of the embryonic left ventricle gives rise eventually to no more than the septal part of the definitive left ventricle [20]. The umbilical vein, which occupies the boundary of embryonic disk and amnion, and the vitelline plexus, which is situated on the yolk sac, merge

at the level of the 4th somite to form the hepatocardiac channels [29]. These channels, in turn, join the systemic venous inflows to the heart. At this stage, both arms of the cardiac inflow tract are transversely oriented vessels, merging in the midline (Figure 2). This site of union represents the caudal continuity between the first and second heart fields [30], and corresponds with the future atrioventricular junction [31]. It is not yet possible anatomically to identify specific venous tributaries, but the primordiums of the atrial chambers are visible. Cardiac jelly forms a thick cuff around the single endocardial tube, while the outer myocardial wall surrounds the jelly as a cloak, which is open dorsally as the dorsal mesocardium. The dorsal mesocardium connects the heart with the overlying pharyngeal floor, while the transverse septum supports the embryonic ventricle caudally (Figure 2).

The lumen of the heart resembles that of an hourglass (Figure 2, upper panel, and Figure 3). At the narrowest part of the hourglass, the dorsal mesocardium has disappeared. At this site, the transverse pericardial sinus, identifiable by the interruption of the dorsal mesocardium in Figure 2 (lower panel), marks the transition from the descending, or inlet, to the ascending or outlet limb of the forming cardiac loop. This junction between the embryonic left ventricle and the forming embryonic right ventricle will eventually be the location of the interventricular foramen. It is at this position, furthermore, that the heart tube bends leftward and, in particular in its cranial part, ventrally (Figure 3).

The looping of the heart brings out the separation of the second heart field into caudal and cranial portions [32]. The caudal second heart field gives rise to both atrial chambers at CS10-11, and the systemic venous sinus at CS12 ([22,33]; Table 1). The cranial second heart field gives rise to outlet limb of the cardiac loop, the proximal portion of which becomes the embryonic right ventricle at CS10, while the distal portion becomes the myocardial outflow tract at CS11 ([24,34]; Table 1). The embryonic right ventricle originates from myogenic cells in the second heart field, which also give rise to the muscles of the 1st pharyngeal arch, whereas the outflow tract is covered by cardiomyocytes, which originate in similar fashion from myogenic cells in the 2nd pharyngeal arch [35,36].

The outflow tract, at the arterial pole, continues extrapericardially as the paired ventral aortas, which extend parallel to the pharyngeal floor in cranial direction. They then pass perpendicularly to the pharynx, in front of its widening part, which will give rise eventually to

the pharyngeal pouches, to join both dorsal aortas. Ventral aortas are found in embryos of all higher vertebrates [37,38], including human embryos during CS10 and CS11. The cranial boundary of the cardiac jelly coincides with the transition of the outflow tract to the ventral aortas. The dorsal aortas course caudally between the dorsolateral wall of the pharynx and the somites, breaking into a plexus where somites are forming. By this stage, the roots of the first pair of intersegmental arteries can be recognized between somites #1 and #2.

Table 1. The early heart grows by the serial addition of cells from the caudal and cranial second heart field. The first structure to develop is the embryonic left ventricle, which forms in late CS9 or early CS10 embryos. Subsequently, the common atrium and embryonic right ventricle form in late CS10 or early CS11 embryos. Myocardial expansion of the early heart is completed at CS11 and CS12, when the myocardial outflow tract and the venous sinus are added. The non-myocardial arterial component of the heart forms at CS15, when the aortopulmonary septum divides the aortic sac into the ascending aorta and pulmonary trunk.

structure	tissue	appearance	boundaries	alternate names	adult name
venous sinus	myocardial	CS12	systemic veins	sinus horns	coronary & systemic venous sinus; sinus node
			venous valves		
R & L atriums	myocardial	CS10-11			
			atrioventricular canal		
embryonic LV	myocardial	CS9-10			left ventricle
			interventricular foramen		
embryonic RV	myocardial	CS10			right ventricle
			narrowing lumen & transition trabeculations-to-endocardial ridges		
proximal OFT	myocardial	CS11		prox. myocardial OFT	infundibulum (R) & aortic vestibule (L)
			dog-leg bend		
middle OFT	myocardial	CS12		distal myocardial OFT	L & R arterial roots
			distal boundary myocard		
distal OFT	non-myocardial	CS15		ascending aorta & pulmonary trunk	intrapericardial arterial trunks
			pericardial reflection		
not part of heart	non-myocardial	CS15		aortic arch & brachiocephalic trunk	extrapericardial arterial trunks

Carnegie Stage 11. Human embryos reach the 11th Carnegie stage when ~29 days have passed since fertilization [13]. The reconstructed specimen is shown in Supplemental Figure 4. It has developed 13 pairs of somites. The neural plate has partially transformed into a tube, with its neuropores reaching the mesencephalon cranially, and the somitomeres caudally to somite #13, which is equivalent to vertebral level T2. The pharynx by now extends further cranially and has widened, but has not, as yet, given rise to individual pouches. The pericardial cavity extends between the stalk of the yolk sac and transverse septum caudally, the pharynx dorsally, and the forebrain cranially (Figure 1). The entire cardiac tube, except for its caudal non-myocardial inflow tract, is invested in cardiac jelly and has myocardial walls (Figure 2, lower

panel). At the venous pole, the hepatocardiac channels, formed from the vitelline and umbilical veins, drain into the inflow tract (Figure 2, upper panel). Together, the hepatocardiac channels and the inflow tract determine the contour of the cranial intestinal portal. Although the cardinal veins have begun to form within the embryo, their connections with the venous pole of the heart have yet to form. A left proepicardial organ can be seen at the junction of the left hepatocardiac channel and the inflow tract.

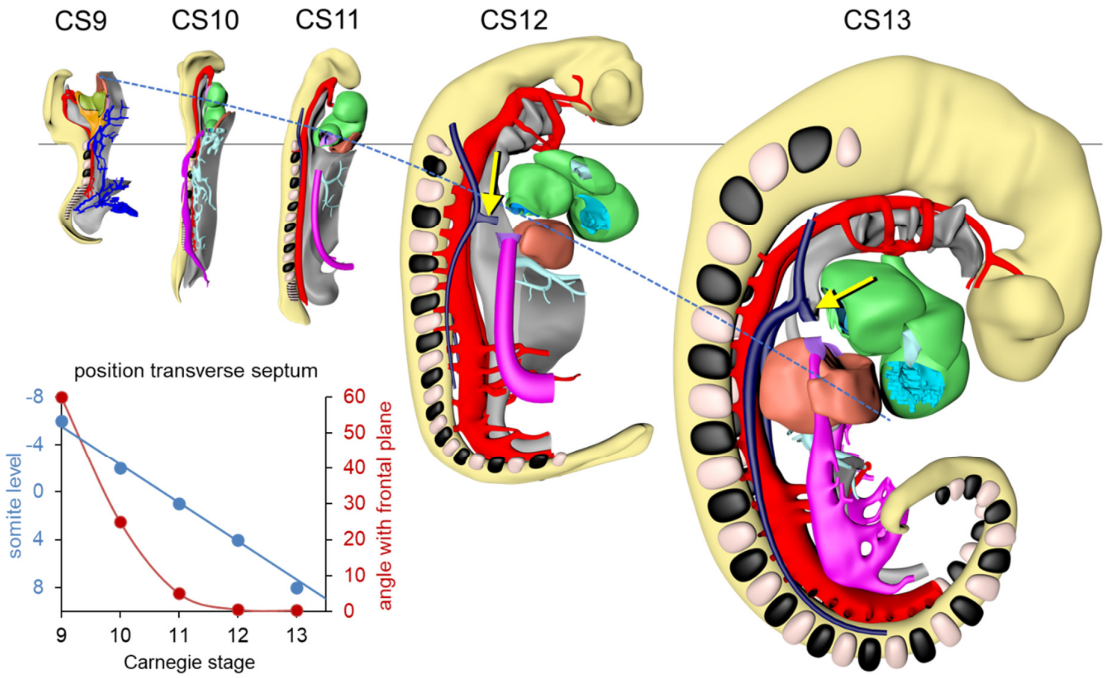

Figure 1: Pictorial timeline of the 'descent" of the transverse septum. Between CS9 and CS13, the transverse septum and, along with it, the heart acquires a progressively more caudal position relative to the body axis due to growth of dorsal structures, such as the neural tube. The horizontal line shows how we aligned all embryos on the position of the first somite. The second, broken, line passes through the middle of the transverse septum. We partially removed some organs to better visualize the septum. The curvature of this line reflects the increasing size of the somites. We determined the position of the transverse septum by placing a line through the center of the septum perpendicular to the curvature of the body axis. This position relative to the first somite is then expressed in the number of somites, a negative number indicating that the septum is situated cranially to the first somite. The blue symbols in the graph show that the position of the septum "moves" caudally at ~3 somite lengths per developmental stage, while the brown symbols show that the position of the septum rotates in a frontal plane across ~60° between CS9 and CS11. The direction of the common cardinal vein (yellow arrow) changes from being oriented transversely at CS12 to achieving a frontal position at CS13, this change also reflecting the descent of the heart. All images are also available as preset views in the corresponding 3D-PDFs.

The expansion and the medial fusion of the myocardial walls of the atriums (Figure 2, lower panel; [39]) are indicative of continuing differentiation. The beginning of ballooning of the right atrium, and the leftward transfer of the atrioventricular canal permit the recognition of laterality

(Figure 2; [32,40]). This laterality involves differences in both the lineage [22] and phenotypic properties [33,41] of the right and left atriums. The apical part of the embryonic left ventricle is also beginning to balloon at the outer curvature of the loop. The outflow tract still bifurcates just ventral to the pharynx into the ventral aortas, which continue dorsally on either side of the pharynx to join the dorsal aortas.

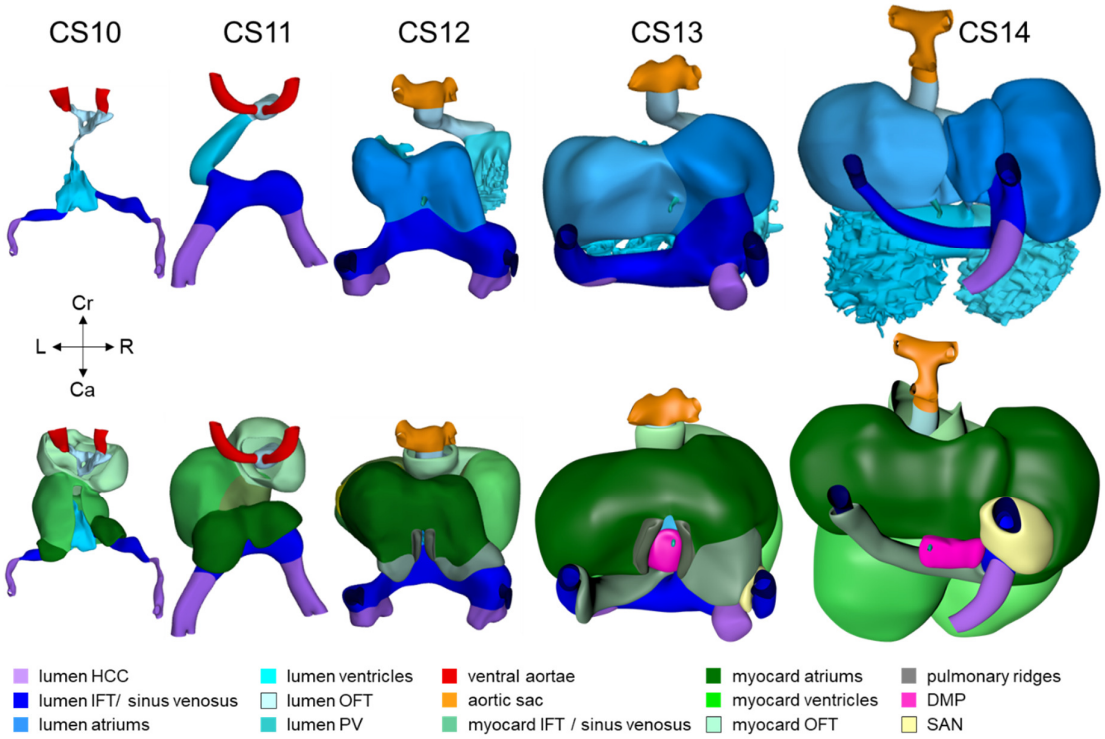

Figure 2: Pictorial timeline of the development of the inflow tract. Dorsal views of embryonic hearts are shown between CS10 and CS14, with the upper panel emphasizing endocardial continuity and the lower panel the myocardial coat. The panels are aligned relative to the position of the pulmonary vein (black horizontal line). Note that the distance between the arterial and venous poles of the heart loop does not change during cardiac looping (CS10-CS12; [42,43]). The appearance of a myocardial wall indicates the formation of that compartment in the inflow tract. Myocardium appears in the wall of the atrium at CS10 and in the wall of the systemic venous sinus at CS12. The pulmonary vein, along with its flanking atrial ridges, also begins to form at CS12. The sinus node becomes recognizable as a separate structure at CS13. The left and right atriums are already distinguishable at CS10, but the sinuatrial junction does not become a right-sided structure until CS13. The atrial septum appears at CS14. It is identifiable as the "empty" space between left and right atriums in the upper panel). The hepatocardiac veins are the only source of venous blood for the heart until CS12, when the initially small common cardinal veins appear. All images are also available as preset views in the corresponding 3D-PDFs.

An early feature, indicating the beginning of cardiac looping, was the appearance of the transverse pericardial sinus in CS10 embryos. The accompanying rightward tilt of the arterial pole, and the leftward tilt of the embryonic left ventricle, are further overt and early signs of asymmetry in these early embryonic hearts (Figure 3 and Supplemental Figure 3). In mice at a

similar stage of development, growth in the left side of the arterial pole, the ventral side of the loop, and the right side of the venous pole, exceeds that in the corresponding opposite sides [43-45]. These findings suggest that the breaking of symmetry during looping results from the asymmetric distribution of cell-proliferation centers [42,43]. Due to a higher rate of proliferation and myocardial differentiation of mesenchymal cells in the dorsal mesocardium [46,47], and their subsequent insertion into the venous and arterial poles of the heart [24,43,48,49], the length of the limbs of the cardiac loop increases between the left atrium and the arterial pole, in particular in its cranial outlet segment (Figure 3; wire frame in Supplemental Figure 4; [43]). At the venous and arterial poles, the heart retains its midline connections with the pharyngeal mesenchyme through the remaining parts of the dorsal mesocardium.

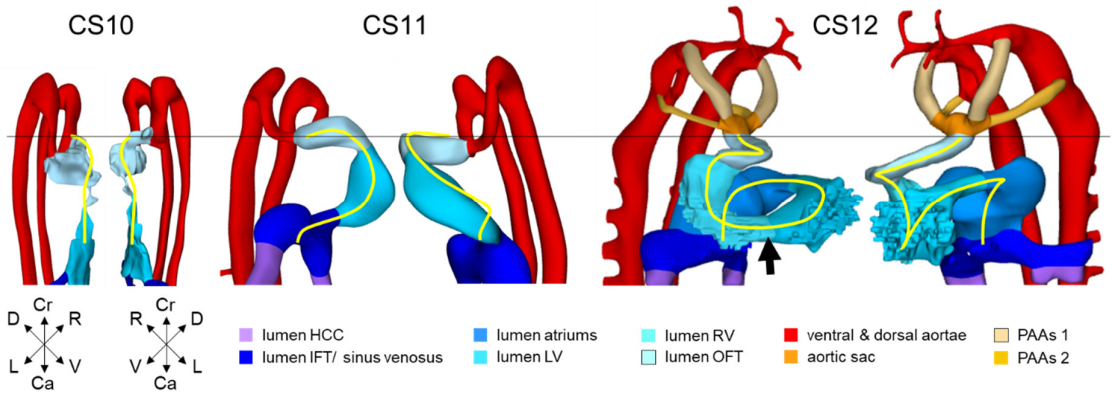

Figure 3. Looping of the heart tube. The panels show ventral right and ventral left views of the cardiac lumen and the adjacent vessels in CS10-12 embryos. The panels were aligned on the arterial and venous poles of the heart loop (black horizontal line). The first signs of looping are seen at CS10, when the dorsal mesocardium disappears at the junction of the embryonic ventricle and outflow tract. The center of the heart tube, represented by the yellow wire, bends leftward and ventrally, in particular in its cranial part. At CS11, the loop extends ventrally due to axial growth and becomes more pronounced, producing the so-called "C"-loop. The embryonic left ventricle represents the most ventral portion of the heart loop at this stage. The atrioventricular junction has moved leftward, while the common atrium and distal part of the outflow tract remain midline structures. At CS12, endothelial sprouting into the cardiac jelly marks the boundaries of the ballooning apical parts of the ventricles (arrow). The heart loop between the left ventricle and distal outflow tract further increases in length in a rightward and dorsal direction, with the embryonic right ventricle emerging at its apex (see wire loop). Note that looping has induced two helical twists in the heart axis that meet in the right ventricle. All images are also available as preset views in the corresponding 3D-PDFs.

Carnegie Stage 12. Approximately 30 days have now passed since fertilization [13]. The reconstructed specimen is shown in Supplemental Figure 5. The cranial neuropore has closed, while the caudal neuropore is now distal to somite #23, which is equivalent to vertebral level T12. The fore- and hindgut have further elongated. The first 2 pharyngeal pouches have formed

in the foregut. The buccopharyngeal membrane is breaking up. Surrounded by the pericardial cavity, the heart itself is now enclosed on three sides by the transverse septum, the pharynx, and the forebrain (Figure 1). The large systemic veins are still bilaterally symmetrical, and common cardinal veins have now formed. Already, the right-sided systemic venous sinus is expanding more rapidly than its left-sided counterpart (Figure 2). Coelomic cells have formed proepicardial organs bilaterally just cranial and lateral to the inflow tract [50]. A still blind mid-pharyngeal strand, which will eventually canalize to form the common pulmonary vein, can be recognized penetrating the dorsal mesocardium between the arms of the inflow tract (Figure 2). The atrial margin of the mesocardium is now flanked by paired mesenchymal ridges (Figure 2, lower panel). Growth of the right-sided ridge, and its fusion with the primary atrial septum, will eventually commit the common pulmonary vein to the cavity of the left atrium [51-54]. The atrioventricular canal has become recognizable, connecting the left side of the atrial components with the embryonic left ventricle.

Axial growth increases the length of the heart loop, placing the ventricles in a ventral position relative to the atriums, whereas radial growth results in the ballooning of the atrial appendages and apical ventricular components [49,55]. The ballooning was first seen in the right atrium and left ventricle of CS11 embryos (Figure 2, upper panel). It results from localized increases in cell proliferation in the outer curvature of the heart loop [5,32,40,56]. The primary myocardium of the embryonic heart is typically bilayered, with a network of thin myocardial strands connecting the layers. The spikes that decorate reconstructions of the lumen of the embryonic left and right ventricles arise from the muscular trabeculations that appear in the ballooning portions of the ventricles between CS12 and CS15 (Figures 3 and 4). In the embryonic left ventricle, trabeculation of the myocardial wall starts with a few endocardial sprouts penetrating the jelly at CS11. The sprouts increase in number and extend into the inner layer of the bilayered primary myocardium at CS12. At CS13, the sprouts spread laterally between both myocardial layers, inducing rearrangement of the inner myocardial layer into radial trabeculations. These muscular columns, temporarily covered by “bubbles” of jelly-like extracellular matrix, expand radially during CS14. Their resorption terminates trabecular growth at CS15 [57]. The outward and radial growth of the trabeculations leaves intact the contours of the original ventricular endocardial tube [5].

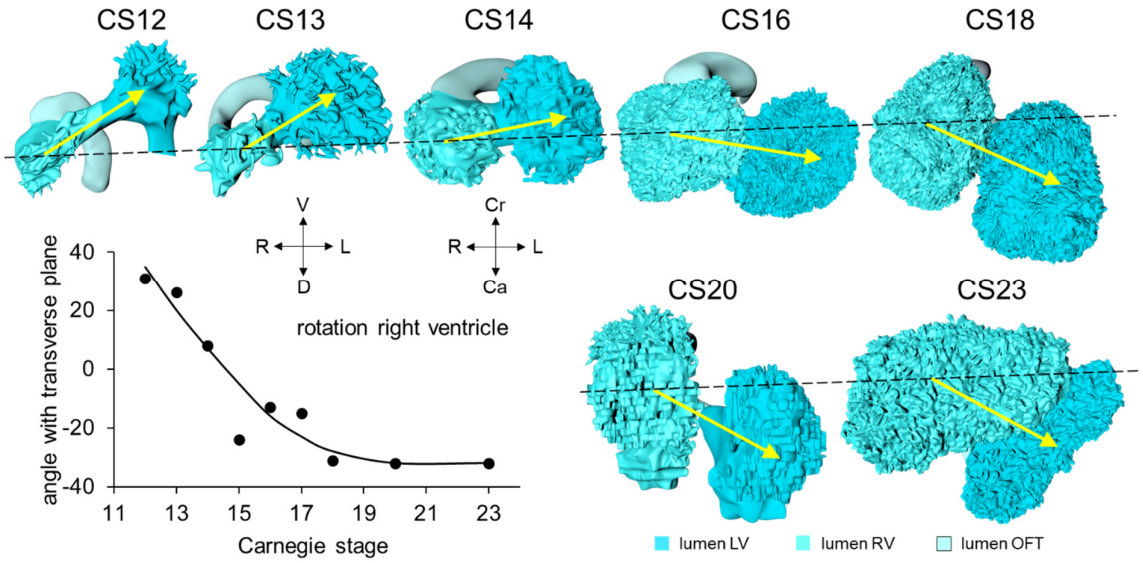

Figure 4: Pictorial timeline of the changing position of the developing right ventricle. The figure shows caudal (CS12 and CS13) or ventral views (CS14-23) of the heart lumen between CS12 and CS23. The difference in the viewing angle reflects the changing curvature of the embryonic axis. The position of the right relative to the left ventricle gradually changes over ~60° between CS12 and CS18 (graph). The right ventricle is positioned caudally relative to the left ventricle at CS12 and achieves a more cranial position after CS18. The interventricular foramen is relatively long during CS12-14. The wide space between left and right ventricular lumens after CS20 reflects the appearance of compact myocardium and a thick muscular ventricular septum. The ventricular axes are almost sagittal prior to CS20, and become oblique and leftward at CS23, reflecting the changing shape of the rib cage [58]. All images are also available as preset views in the corresponding 3D-PDFs.

The appearance of endocardial sprouting into the cardiac jelly marks the morphological formation of the embryonic right ventricle at the apex of the heart loop, and in a dorsal position relative to the left ventricle (Figure 3). The endocardial sprouts also demarcate the left and right boundaries of the interventricular foramen. The size of the cavity, and its trabecular development, are delayed by ~2 Carnegie stages in the embryonic right relative to the embryonic left ventricle (Figure 4). Differential expression of transcription factors, including *Hand1* and *-2* [59], and *Tbx1* and *-5* [32,60], sustains the differences in growth and shape of the left and right ventricles. The embryonic right ventricle continues distally into the smooth-walled myocardial outflow tract. Separate left and right bloodstreams now already become visible in the outflow tract [61,62]. Since the inner curvature of the heart does not participate in ballooning and trabeculation, the boundaries of the respective cardiac compartments can only be distinguished along the outer curvature.

When the second heart field starts to contribute cells to the arterial pole of the heart [32,63], the walls of the loop take a helical path between the atrioventricular canal and distal outflow tract (Figure 3; wire frame in Supplemental Figure 5; [40,64]). This helical configuration can be shown by the expression pattern of the left-sided marker *Pitx2c* [65,66], by lineage tracing [35,40,67] and by the course of the endocardial ridges formed in the outflow tract [7,68]. The walls of other structures that form loops, such as the intestines [69], follow strikingly similar courses. During this phase of looping, the elongating muscular outflow tract forms an acute bend between its transversely oriented proximal part, which is also known as the "conus", and its ventrodorsally oriented distal part, also known as the "truncus" [8]. The pronounced "bayonet" [70] or "dog-leg" bend [71] between these parts marks the junction. This bend may be a critical structural element for effective valveless pumping in these early hearts [72]. The presence of the bend permits the outflow tract to be described as having proximal and middle parts, which are myocardial, with the non-myocardial distal part being added when the arterial trunks begin to form in CS15 embryos (Table 1).

By this stage, it is possible to recognize the first two pharyngeal arches, along with their accompanying arteries. The vascular space within the ventral pharyngeal mesenchyme that connects the outflow tract with the arteries of the pharyngeal arches is known as the aortic sac. The endothelium of the first two pharyngeal arches shares its lineage with that of the dorsal and ventral aortas, but differs from that of the subsequent pharyngeal arch arteries [73]. The dorsal aortas have fused between somites #10 and #13 (vertebral levels C6-T2), and continue cranially into the carotid arteries.

Carnegie Stage 13. This stage, reached at ~32 days after fertilization [13], is considered "phylotypic". This is because morphologic features and profiles of gene expression are most similar among vertebrate embryos at this stage [15]. The reconstructed specimen is shown in Supplemental Figure 6. Due to dorsal growth in its sacral region, first noticeable at CS12, the embryonic body axis assumes a helical shape, with the tail region typically on the right side of the body [74]. The heart, within its pericardial cavity, remains surrounded by the transverse septum, the pharynx, and the forebrain. Due to the rapid growth of the brain and foregut between CS9 and CS14, the transverse septum gradually changes in orientation from frontal at CS9 to near-transverse at CS11 (Figure 1). It also "descends" from ~6 somite lengths cranial to the first somite at CS9 to somite #8 at CS13, representing ~3 somites per developmental

stage (Figure 1, graph). The large caudal veins remain symmetrical in terms of their size [69], but the vitelline veins have by now been incorporated into the developing liver [29]. The course of the common cardinal veins has changed, following the elongation of the foregut, from being transverse to longitudinal (Figure 1). It is no longer possible to recognize the proepicardial organs, but epicardium is now spreading over the surface of the heart, accumulating in the atrioventricular and interventricular grooves. We show only the thick layer of epicardium in the grooves in our reconstructions.

Myocardium has appeared on the epicardial side of the asymmetrically expanding systemic venous sinus, permitting the definition of the sinus horns (Figure 2, lower panel; [75]). The myocardial walls of the horns differ from those of the atrial chambers and the pulmonary vein in developing from an *Nkx2-5*-negative, *Tbx18*-positive lineage [22,23,39,41,75]. By this stage, furthermore, the systemic venous sinus drains exclusively into the right side of the atrial chambers through the right-sided sinuatrial junction (Figure 2, upper panel). The stem of the solitary pulmonary vein now exits the left atrium through the dorsal mesocardium, but is still blind-ending (Figure 2, lower panel; [52,53]). Between CS12 and CS13, a subpopulation of endocardial cells undergoes endocardial-to-mesenchymal transformation and colonizes the endocardial jelly [76,77]. This results in the appearance of cellularized endocardial cushions superiorly and inferiorly within the left-sided atrioventricular canal, with the cushions having atrial extensions that encircle the wide interatrial junction. This junction is known as the primary atrial foramen. The myocardial trabeculations remain more advanced in the embryonic left than the right ventricle, while the muscular ventricular septum is no more than a shallow ridge. The cavity of the outflow tract remains surrounded by endocardial jelly, with its smooth-walled myocardial wall extending distally to reach the pericardial reflections. The lumen of the outflow tract then continues via the aortic sac and arteries of the pharyngeal arches to the paired dorsal aortas. There are now 3 pharyngeal pouches, which interpose between 4 arches. The 1st pair of pharyngeal-arch arteries has disappeared, whereas arteries have formed in the 3rd and 4th arches.

Carnegie Stage 14. The embryo has now been developing for ~34 days subsequent to fertilization [13]. The reconstructed specimen is shown in Supplemental Figure 7. Since the cranial somites are no longer identifiable, we revert to spinal ganglia as our reference for segmental level. By this stage the left hepatocardiac channel has disappeared [29], while the right

hepatocardiac channel has become part of the inferior caval vein (Figure 2). The confluence of the cranial and caudal cardinal veins has substantially increased in diameter on both sides, while both sinus horns have completely myocardialized. The primordium of the sinus node, with an obvious tail [78], is recognizable as a myocardial cuff at the junction between the right atrium and right common cardinal vein (Figure 2, lower panel), which itself is now recognizable as the superior caval vein. In mice, the left-sided marker *Pitx2c* suppresses development of a sinus node along the left common cardinal vein [41].

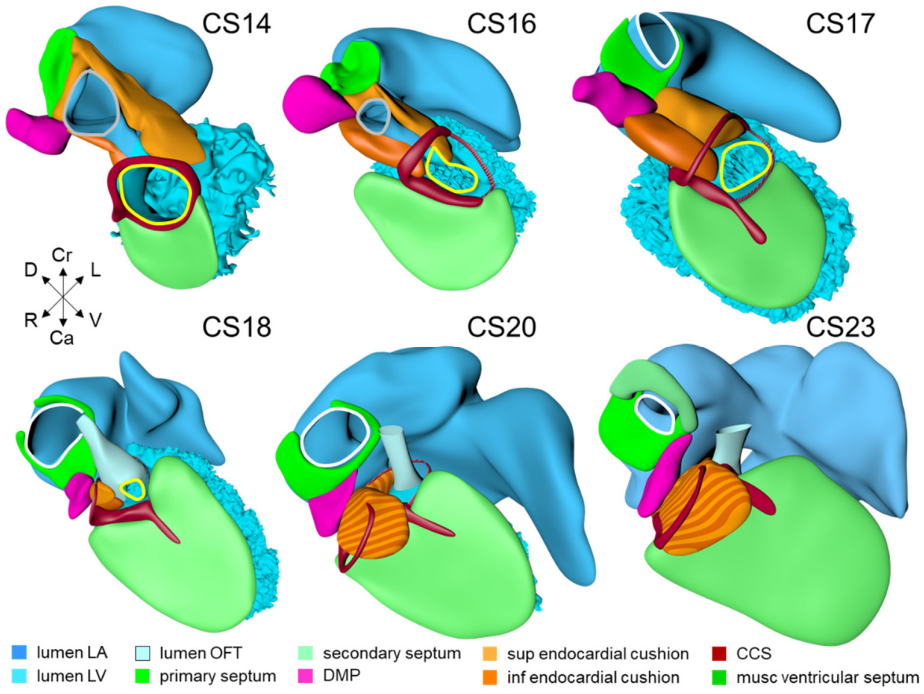

Figure 5: Pictorial timeline of the closure of the interatrial & interventricular foramens. The panels show right ventral views of the left side of the heart. The left atrial and ventricular cavities, the muscular atrial and ventricular septums, the endocardial cushions, the dorsal mesenchymal protrusion, the secondary atrial septum (CS23 only), and the GlN-positive ring bundle are shown. The superior and inferior endocardial cushions fuse at CS17, entailing the concomitant closure of the primary atrial foramen and the appearance of a very wide secondary atrial foramen. The dorsal mesenchymal protrusion acquires a position at the base of the atrial septum due to expansion of surrounding structures. The protrusion muscularizes, along with the mesenchymal cap, starting at CS18, and concomitant with the proximal endocardial ridges of the outflow tract. The borders of the interventricular foramen remodel as revealed by the course of the GlN-positive ring. As soon as septation of the outflow tract is complete at CS18, the myocardialized part of the fused endocardial ridges and the rightward margins of the atrioventricular endocardial cushions combine to decrease the size of the remaining foramen. Closure is complete at CS20. Gray contours: primary atrial foramen; white contours: secondary atrial foramen; yellow contours: interventricular foramen. All images are also available as preset views in the corresponding 3D-PDFs.

The sinuatrial connection, now narrow, is guarded by the venous valves. These valves merge into the spurious septum craniodorsally, and attach in the primary myocardium of the atrial floor caudoventrally. The primary atrial foramen remains surrounded by the atrial extensions of the superior and inferior atrioventricular cushions, with the extension of the superior cushion being a mesenchymal cap on the leading edge of the newly-developing primary atrial septum (Figure 5; [79]). The pulmonary vein, which passes between the atrial extensions of the atrioventricular cushions and through the dorsal mesocardium, has now canalized so as to connect with the venous plexuses developing ventral to the lung buds. The rightward margin of the dorsal mesocardium (Figures 1, lower panel, and 5) is known as the vestibular spine [53] or, more recently, the dorsal mesenchymal protrusion [54]. The atrioventricular canal itself is surrounded by bilayered primary myocardium that extends in the atrial floor to the root of the pulmonary vein and the base of the right venous valve. The cushions within the canal now divide its lumen into narrow left and right atrioventricular passages, but have yet to fuse.

The trabeculated free walls of the ventricles continue their ballooning. The left ventricle expands by recruiting cells from the atrioventricular canal [20,80,81], while the right ventricular trabeculations have begun to extend at the expense of the proximal outflow tract [82-84]. With the ballooning of the ventricular compartments, it is now possible to recognize the muscular ventricular septum (Figure 5; [85,86]), with evidence of cell multiplication at its base [87]. Its crest forms the caudal margin of the interventricular foramen, with the inner curvature forming the cranial margin (Figure 5). The myocardium surrounding the interventricular foramen, which is the first component of the second heart field to differentiate [81], can be stained with the "GlN2", "Hnk1", or Leu7 monoclonal antibodies [88]. All of these antibodies recognize a terminal 3-sulfated glucuronic-acid epitope on macromolecules [89]. The very dense appearance of the myocardium of this interventricular ring also makes possible identification of its components in routine histological sections [90,91].

The development of a physical separation between the systemic and pulmonary circulations is known as "septation". In early embryonic hearts of mice [92] and chicken [61,62,93,94] blood flow is laminar, which limits its mixing. With the appearance of ventricular trabeculations during CS13-14 [5,56,95,96], conduction velocity through the myocardial walls increases, and the activation of the ventricle changes from a base-to-apex to an apex-to-base sequence [97-99]. Cardiac pumping, furthermore, switches from a suction, or impedance, to a pulsatile, or piston,

mechanism [100]. Because cardiac output increases [101], vortical patterns of streaming [102] and mixing develop, especially downstream of the relatively narrow and still slowly contracting atrioventricular canal and outflow tract [61,94]. The temporal correspondence of the increasing functional effectivity of embryonic hearts [103-105], and anatomical septation, therefore, is not coincidental.

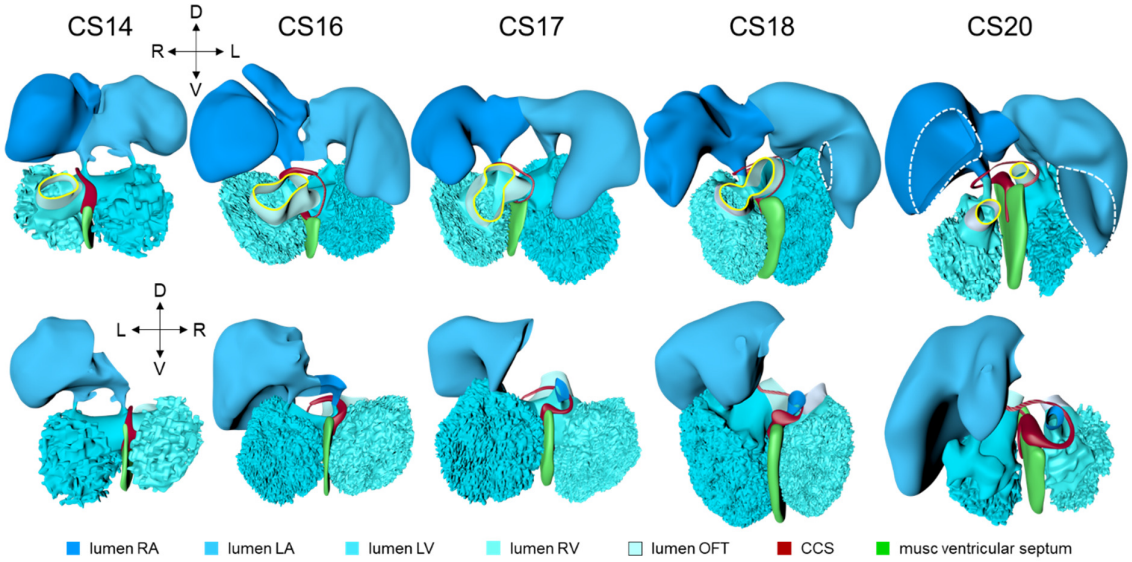

Figure 6: Pictorial timeline of the subdivision of the interventricular foramen into the peri-tricuspid inlet, subaortic outlet, and membranous septum. The figure shows the lumens of the atriums, ventricles and outflow tract, and the muscular ventricular septum. The upper panels show the cranial view, and the lower panels the caudal view. When first formed, the interventricular foramen is a sagittally oriented interventricular conduit, as visualized by the GlN-positive ring. The craniodorsal part of the foramen, from which the GlN fades away at CS16, is indicated by a thinner, hatched line. The tips of the atrial appendages are clipped in the images for CS18 and CS20 (dashed lines) to permit inspection of the atrioventricular junction and outflow tracts. At CS16, the caudal part of the foramen and GlN ring begin to expand in rightward direction, producing a direct connection between the right atrium and ventricle, which is best seen in the lower panel. Meanwhile, the cranial, subaortic part of the foramen, which is best seen in upper panel, gradually expands craniodorsally. Comparing the arrangements at CS18 and CS20, when the septation of the outflow tract is complete, shows that the subaortic, but not the subpulmonary, ventricular outlet is surrounded by the GlN ring. The remaining connection between right ventricular cavity and the subaortic channel is still present at CS18. It is obliterated at CS20 by formation of the membranous septum (not itself visible). All images are also available as preset views in the corresponding 3D-PDFs.

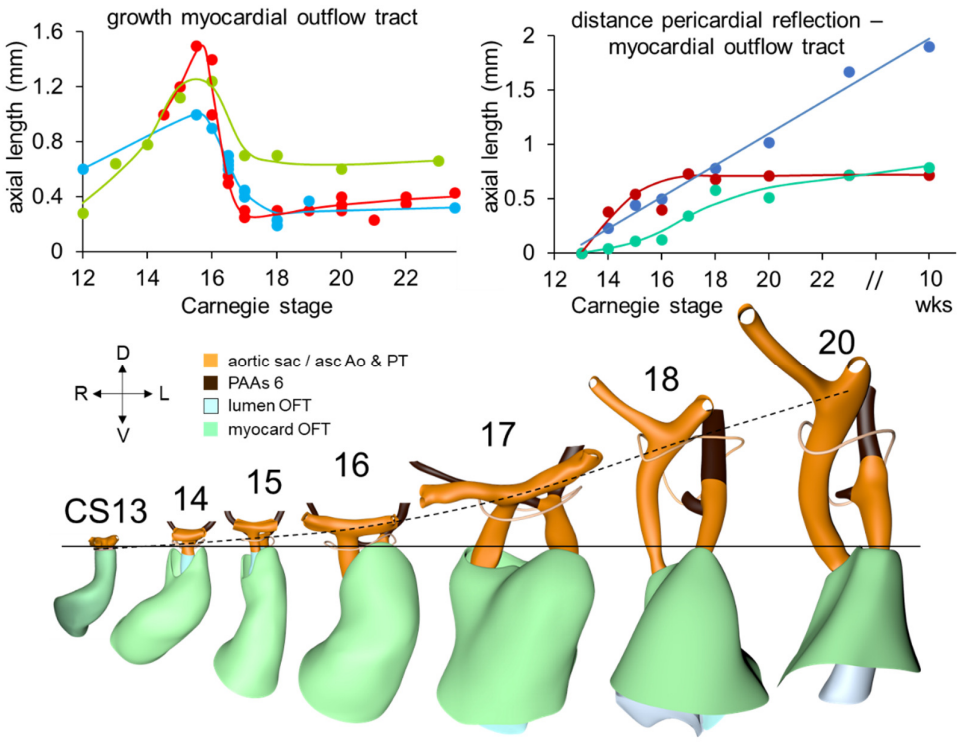

Figure 7. Changes in size and shape of the myocardial outflow tract and arterial trunks. The left-sided graph shows the length of the muscular outflow tract between the proximal and distal ends of the endocardial outflow ridges. The green symbols represent the measurements made in our reconstructions, with the blue symbols taken from measurements made in 14 scanning electron microscopic images [106], and red symbols representing those made in 18 immunohistochemically stained and partially reconstructed hearts [107]. There is axial growth of the muscular outflow tract up to CS16, when its length suddenly declines profoundly, with no resumption up to CS23. The right-sided graph shows the axial growth of the arterial trunks. The ascending aorta (blue) increases continuously in length between CS14 and 10 weeks of development, whereas axial growth of the pulmonary trunk (red) stops after CS17. The distance between the distal myocardial border and the pericardial reflection (green) increases little to CS16, indicating that the myocardial jaws of the fishmouth stay close to the pericardial reflection. Concomitant with the abrupt shortening after CS16, the myocardial border moves away from the reflection. The lower panel shows cranial views of the myocardial outflow tract, the arterial trunks, with 6th arch and pulmonary arteries, and the pericardial reflection (wire loop). The images are aligned to the distal myocardial border of the outflow tract (black line). The dashed black line shows the axial growth of the aortic trunk (also shown in Figure 8). The slits in the jaws of the myocardial fishmouth are occupied by the non-myocardial mural tissues (not shown, but see Figure 9, upper row). All images are also available as preset views in the corresponding 3D-PDFs.

Septation proceeds centripetally from the venous and arterial poles towards the interventricular foramen. Septation of the inflow tracts becomes feasible once the systemic venous sinus and its tributaries are committed to the developing right atrium, and the pulmonary vein is committed to the developing left atrium. This is seen in CS13 embryos (Figure 2). The primary atrial septum begins to form at CS14 (Figures 2, upper panel, and 5), followed by functional

454 septation of the atrioventricular canal by the endocardial cushions into left- and right-sided
455 channels. The borders of the interventricular foramen become remodeled eventually into peri-
456 tricuspid and peri-subaortic portions. These are then separated anatomically by the formation
457 of the membranous septum, which closes the middle portion of the initial foramen at CS20. It
458 is the residual primary myocardium in the inner curvature of the heart that becomes modified
459 during these processes [108]. The expression of GlN in the myocardium surrounding the
460 interventricular foramen facilitates the description of the changes in its shape during the process
461 of septation. Until the end of CS15, however, it remains a flat and round entity, with its borders
462 well described as the primary ring (Figures 5 and 6).
463
464 Septation of the outflow tract proceeds from the aortic sac towards the interventricular foramen.
465 At CS14, the arteries of the 2nd pharyngeal arch have disappeared, while the arteries of the 6th
466 pharyngeal arch have formed. Although only 5 pharyngeal arches form in amniotes [109], it
467 remains conventional to describe the ultimate arches as being the 6th entities. The pulmonary
468 arteries have yet to appear in this embryo. The mesenchyme of the pharyngeal arches derives
469 from the neural crest [110], whereas the endothelium of pharyngeal arch arteries 3, 4 and 6 derives
470 from the second heart field [73]. Due to its slow proliferation [48,111] the distal part of the myocardial
471 outflow tract becomes relatively shorter than its proximal part (Figure 7, lower panel). Up to
472 and including CS13, the distal myocardial boundary reaches to the pericardial reflection, with
473 a thick acellular layer of endocardial jelly surrounding the lumen of the outflow tract. At CS14,
474 the cells derived from the cardiac neural crest (Figure 8, lower panel and Figure 9, upper panel)
475 and columns of non-myocardial mural cells (Figure 9, upper panel) appear as new structures
476 that transform the architecture of the aortic sac and the distal outflow tract.

477 Cells derived from the neural crest, which surround the arteries of the pharyngeal arches, begin
478 to indent the dorsal wall of the aortic sac. They form a protrusion between its cranial portion,
479 which connects to the arteries of the 3rd and 4th pharyngeal arches, and its caudal portion, which
480 connects to the arteries of the 6th pharyngeal arch. The neural crest cells extend ventrally,
481 having embraced the aortic sac bilaterally, and from there invade the endocardial jelly of the
482 outflow tract as prongs of dense mesenchyme [112]. In this way, they remodel the cuff of
483 endocardial jelly into right- and left-sided columns (Figure 8, upper panel; [112,113]). Meanwhile,
484 endocardial cells that undergo epithelio-mesenchymal transformation also populate the
485 endocardial jelly [76,114]. The initially more numerous [68] neural crest cells are necessary for
486 correct positioning of the ridges, and for patterning of the arterial valvar leaflets [113]. The feature,

therefore, that distinguishes these ridges from the endocardial cushions of the atrioventricular canal is the presence of neural crest cells. For this reason, we describe the outflow entities as ridges, rather than cushions. The prongs within the ridges take a clockwise-spiraling course when observed from the right ventricle, occupying septal and parietal locations at their junction with the developing right ventricle (Figures 8, lower panel, and 9, upper panel; [7,68]).

The cranial second heart field produces 2 waves of progenitor cells that are destined to form the outflow tract. The first wave arises at CS10, and contributes to the cranial wall of the muscular outflow tract until CS14 and to the ascending aorta thereafter. The second wave evolves more gradually between CS11 and CS15, and contributes to the caudal wall of the muscular outflow tract and, after CS14, to the pulmonary trunk [115,116]. These cells of the second wave are dorsally continuous with, and probably originate from a phenotypically similar mass of pharyngeal mesenchyme surrounding the trachea [34,117,118]. This "club" of mesenchyme forms during CS13, and remains an identifiable entity during CS14 and CS15 (Figure 9, upper panel). The progenitor cells in the club converge and extend into a procession of cells that moves towards, and then into the relatively narrow outflow tract before locally differentiating [116,119,120]. Convergent extension is mediated by the planar cell polarity pathway [121]. When the addition of new cardiomyocytes ceases at CS14, non-myocardial cells start to form the distal portion of the outflow tract. These cells insert themselves cranially and caudally as columns between the remaining myocardial walls [7,122,123]. Consequently, the distal myocardial boundary takes on a fishmouth appearance (Figure 7, lower panel). In contrast to the caudal, or pulmonary, column, which extends to the peritracheal mesenchymal mass, the cranial, or aortic, column is short when traced into the pharyngeal floor.

In contrast to the neural crest cells, the cells of aortic and pulmonary mural columns do not penetrate the distal endocardial jelly, but maintain an oblique lateral-to medial zone of apposition. Following Tandler [124] and Kramer [8], we will name these endocardial structures "swellings". The cranial, or aortic, swelling differs from the caudal, or pulmonary swelling in that it is invaded by some neural crest cells [113]. The swellings differ from the ridges in that they are initially (CS14 and CS15) confined to a small subsection of the middle portion of the outflow tract near the dog-leg bend (Figure 8). Consequently, the endocardial jelly, which still surrounds the lumen of the outflow tract as a smooth cuff at CS13, reorganizes distally into 4 orthogonal columns, while only two columns persist proximally (Figure 8, upper panel).

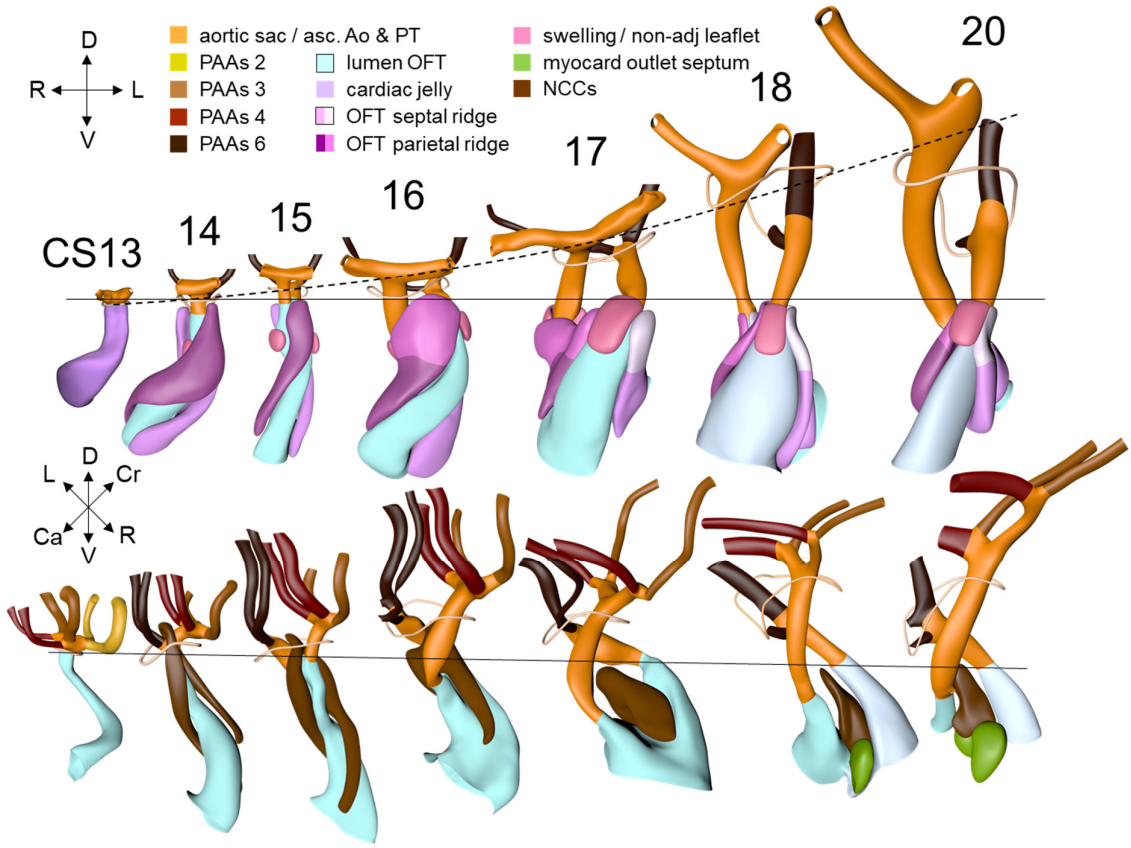

Figure 8. Pictorial timeline of the changes in size and shape of the lumen, endocardial ridges and swellings, and neural-crest prongs of the outflow tract. The images are aligned on the location of the developing pulmonary valve (black line). The upper panel shows cranial views of the outflow-tract lumen flanked by the parietal and septal endocardial ridges, and aortic and pulmonary swellings. The viewing angle is the same as for the lower panel of Figure 7. The arterial trunks are shown for identification of the subaortic and subpulmonary channels. The widening of the distal portions of both outflow ridges during CS16 and CS17 presages their allocation to the right or left semilunar leaflets of the aortic and pulmonary arterial valves at CS18. The valvar portions are marked by a less dark tint of the coding color, and are confined to the distal portion of the myocardial outflow tract. The dashed black line in the upper panel shows the axial growth of the intrapericardial component of the aortic trunks. The saddle-shaped wire loop shows the position of the pericardial reflection. The lower panel shows lumen of the outflow tract as seen from the right side, showing the neural crest cells within the aortopulmonary septum extending as columns of dense mesenchyme into both endocardial outflow ridges. The fusion of these columns creates a temporary "whorl" of neural crest cells between the subaortic and subpulmonary channels. The neural crest cells largely disappear between CS18 and CS23 due to intense apoptosis [125], with invading cardiomyocytes simultaneously populating the shell of the septum [68,126]. All images are also available as preset views in the corresponding 3D-PDFs.

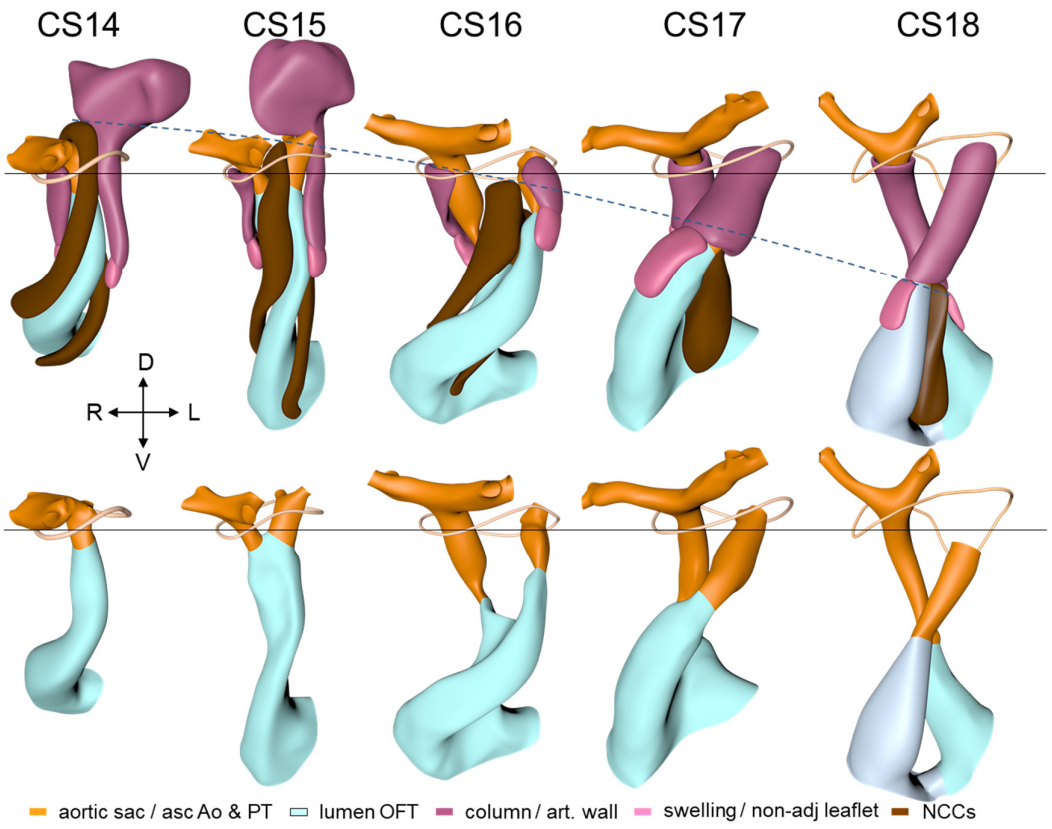

Figure 9: Pictorial timeline of the appearance of the non-myocardial walls of the arterial trunks. The panels are aligned on the pericardial reflection, shown by the wire loops, as in Figure 8. The upper panel shows the lumen of the outflow tract, with the arterial trunks, the columns of neural crest, and the non-myocardial mural columns. The neural crest cells and intercalating non-myocardial tissues invade the distal wall of the outflow tract during CS14. The mural cells are first seen as relatively short aortic or cranial, and pulmonary or caudal columns. During CS14 and CS15, the pulmonary column is continuous dorsally with a club-like condensation of peritracheal mesenchyme, which has disappeared at CS16. The endocardial swellings associated with the aortic and pulmonary mural columns are relatively small during CS14 and CS15, but increase in size from CS16 onwards to begin their transformation into the dorsal and ventral semilunar leaflets, respectively, at CS18. As shown by the interrupted line, there is a gradual increase in the distance between the pericardial reflection and the plane of the valvar primordiums (*cf.* Figure 8). The lower panel shows the same view of the lumens. Note that the prongs of neural crest mesenchyme mold the subaortic and subpulmonary channels during CS15 and CS16. The fusion of these prongs into a central whorl marks the separation of the subaortic and subpulmonary channels during CS17 and CS18. All images are also available as preset views in the corresponding 3D-PDFs.

Carnegie stage 15. At this stage ~36 days have passed since fertilization [13]. The reconstructed specimen, although one of the best CS15 specimens of this stage in the Carnegie collection (http://virtualhumanembryo.lsuhsc.edu/demos/Stage15/Intro_pg/Intro.htm), suffered from venous congestion. Because of this, we reconstructed only its ventricles and outflow tract in detail (Supplemental Figure 8). Compared to the embryo shown for CS14, the

558 changes in the arrangement of the systemic veins, venous sinus, and atrial chambers are limited,
559 as is the arrangement of the pulmonary vein [51-53]. We also found no notable changes in the
560 architecture of the ventricles. The GlN-positive interventricular ring is still a planar structure
561 [127], but a widening of the crest of the muscular ventricular septum identifies the developing
562 branching component of the atrioventricular conduction axis [128].
563
564 CS15 is the most advanced stage in which the arteries within the pharyngeal arches retain their
565 symmetry, albeit that the portions of both dorsal aortas between the arteries of the 3rd and 4th
566 arches, known as the carotid ducts, have markedly decreased in diameter [129]. By this stage, the
567 arteries of the left and right 6th pharyngeal arches have each given rise to a pulmonary artery,
568 which extends caudally within the pharyngeal mesenchyme along the trachea. The most
569 pronounced developmental changes are to be seen in the arrangement of the middle portion of
570 the outflow tract and the aortic sac. Continued axial growth within the myocardial part of the
571 outflow tract (Figure 7, left graph) has all but eliminated the dog-leg bend. The aortopulmonary
572 septum, initially seen at CS14 as a transverse protrusion extending from the dorsal wall of the
573 aortic sac between the origins of the arteries of the 4th and 6th pair of pharyngeal arches, now
574 extends obliquely in a ventral direction towards the distal margins of the endocardial ridges in
575 the middle portion of the outflow tract (Figures 8 and 9, upper panel; [130]). In consequence, the
576 aortic sac acquires a dextrocranial systemic component, which connects the subaortic part of
577 the outflow tract with the arteries of the 3rd and 4th pharyngeal arches, and a sinistrocaudal
578 pulmonary component, which connects the subpulmonary part of the outflow tract with the
579 arteries of the 6th arches (Figures 7-9). The intrapericardial part of the systemic component can
580 be labeled with Mef2c-Cre [131], often used as a marker of the cranial second heart field, and
581 becomes the ascending aorta. The lateral horns of the aortic sac remain unlabeled, and become
582 the extrapericardial part of the ascending aorta, the brachiocephalic trunk, and the initial part
583 of the transverse aortic arch. The pulmonary component becomes the pulmonary trunk, an
584 entirely intrapericardial vessel. It is the ventral growth of the aortopulmonary septum,
585 therefore, which initiates the anatomical separation of the arterial pole of the heart [122,132], along
586 with the formation of the non-myocardial distal portion of the outflow tract. The configuration
587 of the distal myocardial jaws and the interposed mural columns remains unchanged relative to
588 that in CS14. Accordingly, the distal myocardial jaws still extend close to the pericardial
589 reflection (Figure 7, lower panel). As in the CS14 embryos, tissue with the phenotypic property
590 of the pulmonary mural column extends dorsally to the dense mesenchyme that surrounds the
591 trachea (Figure 9, upper panel).

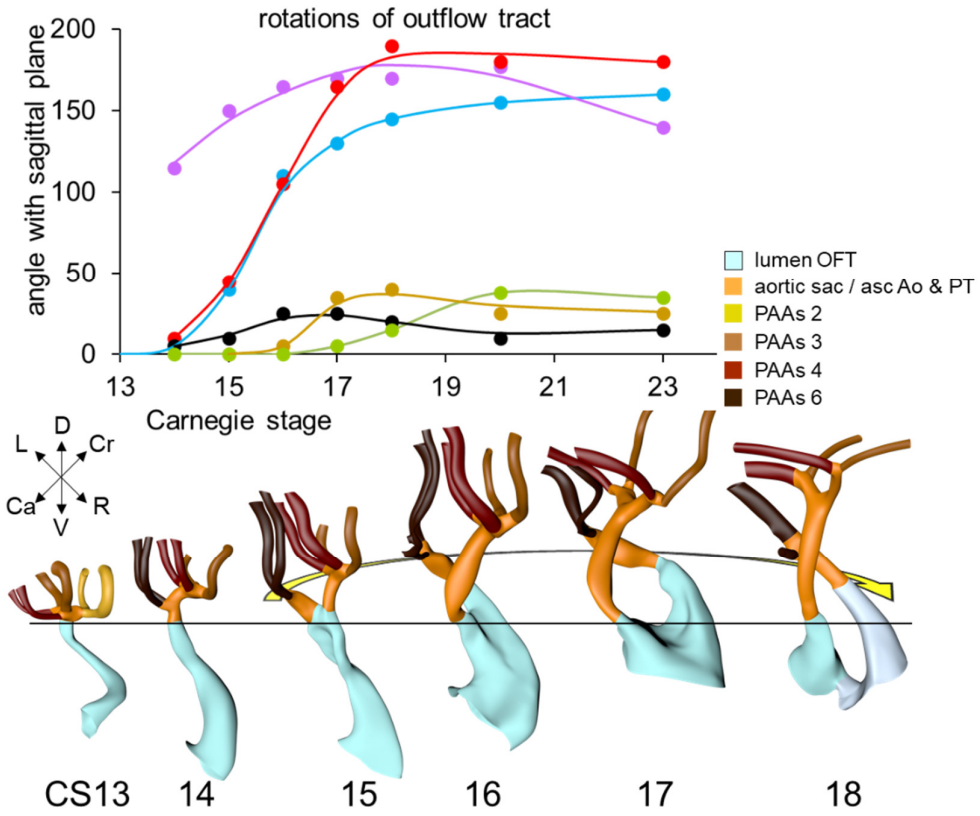

Figure 10: Changes in the course of the (sub-)aortic and (sub-)pulmonary channels. The graph shows the changes in the degree of spiraling of the blood streams in time and place. The reference plane is sagittal. The line connecting the center of the ridges at their proximal ends is shown in purple symbols, with the comparable line at their distal ends shown in red symbols. The blue and black symbols identify the line connecting the centers of the orifices of the ascending aorta and pulmonary trunk at their proximal and distal ends, respectively, with the distal end of the ascending aorta measured at the pericardial reflection. The brown symbols show the movement of the distal endocardial ridges relative to the distal orifices of the subaortic and subpulmonary channels. The green symbols show the asymmetric development of the horns of the aortic trunk measured as the angle of the lines connecting their junctions with the pharyngeal arch arteries. Comparison of the red and purple symbols shows that, by CS17, the endocardial ridges have lost the initial spiraling arrangement identifiable at CS14. The change in orientation of the myocardialized proximal ridges between CS20 and CS23, as they transform into the subpulmonary infundibulum, accounts for the decline in the purple symbols (see Figure 12, upper panel, for morphological details). The compensatory spiraling of the intrapericardial course of the arterial trunks, as shown by the blue symbols, reflects the oblique ventral extension of the aortopulmonary septum, with the black symbols showing that the change in position of the arterial trunks at their connection with the pharyngeal arch arteries contributes to a much lesser extent. The images in the lower panel (same viewing angle as Figure 8, lower panel) are aligned on the location of the developing aortic valve (black line). The horizontal yellow arrow shows the changing position of the (sub-)aortic and (sub-)pulmonary channels in the middle and distal portions of the outflow tract. These channels separate between CS14 and CS15 in the distal outflow tract, during CS16 and CS17 in the middle outflow tract, and between CS18 and CS20 in the proximal outflow tract. All images are also available as preset views in the corresponding 3D-PDFs.

The prongs of neural crest cells, which dorsally are continuous with the neural crest cells in the pharyngeal floor and the aortopulmonary septum [112], can now be traced ventrally into the proximal outflow ridges. By this stage, it becomes possible to recognize the sites of formation of the arterial valves as increasingly narrow passages between the endocardial ridges medially and the swellings laterally [8]. These passages are recognizable histologically by their lining with intensely staining, cobble stone-shaped endocardium. Separate aortic and pulmonary channels are now identifiable in luminal casts of the middle portion of the outflow tract. They extend from the initial site of the dog-leg bend to the distal boundary of the myocardium of the outflow tract (Figure 10, lower panel). Until fusion of both endocardial ridges occurs during CS17, the subaortic and subpulmonary channels remain connected by an aortopulmonary foramen, which is bounded dorsally by the leading edge of the aortopulmonary septum. At this distal location the parietal and septal ridges occupy craniosinistral and caudodextral positions, respectively, with the still small swellings occupying the spaces in between (Figure 9, upper panel).

Carnegie stage 16. This stage is reached at ~38 days after fertilization [13]. The reconstructed embryo is shown in Supplemental Figure 9. The systemic venous sinus, its sinuatrial valves, and the sinus node have largely retained the appearances seen in the previous stage. The pulmonary vein remains a solitary and narrow channel. The primary atrial septum, with its mesenchymal cap, has extended further towards the atrioventricular canal (Figure 5). This reduces the size of the primary atrial foramen, but the atrioventricular cushions still have to fuse. The expansion of the atrial chambers to either side of the outflow tract reveals pronounced growth of the atrial appendages (Figure 6, upper panel). With continuing caudal expansion of the atrium, the right border of the dorsal mesenchymal protrusion expands, like a spine, into the atrial cavity, growing between the atrial surfaces of the superior and inferior atrioventricular endocardial cushions (Figure 5; [133,134]).

The embryonic left and right ventricles are now of similar size and occupy a transverse plane (Figure 4). The changing boundaries of the interventricular foramen can still be followed conveniently in hearts stained for the GlN antigen (Figures 5 and 6). In the inner curvature of the heart, the right wall of the atrioventricular canal continues into the caudal part of the interventricular foramen. Rightward expansion of the confluent part of these structures across the muscular ventricular septum has produced a direct connection between the right atrium and the right ventricle (Figure 6, lower panel; [135]). Subsequently, the cranial portion of the

interventricular foramen will evolve into the channel between the left ventricle and the subaortic outlet (Figure 6, upper panel). At this latter location, however, the primary ring (hatched section) has lost its GlN expression [88], but remains identifiable as part of the central conduction system in birds [136]. In the reconstructions, we have presumed that it lies, as in birds, in the inner curvature at the junction of the left ventricle with the outflow tract.

The length of the myocardial portion of the outflow tract increases ~4-fold in the 8 days between CS12, when it can be first differentiated from the embryonic right ventricle, and CS16 (Figure 7, left-sided graph), underscoring its continuous axial growth. The distal tongues of the myocardial outflow tract still extend close to the pericardial reflection (Figure 7, lower panel), but relative to the diameter of the outflow tract, their length declines. Similarly, the aortic and pulmonary mural columns become relatively shorter. The ascending aorta and pulmonary trunk have also increased substantially in length since their appearance at CS14, but axial growth of the pulmonary trunk ceases after CS16 (Figure 7, right-sided graph). This cessation of growth coincides with, and may reflect, the depletion of the peritracheal cell mass ("club") that is present at CS14 and CS15 (Figure 9, upper panel). At this stage of development, separate flows of blood reach the systemic and pulmonary arch arteries [7,11], but the endocardial outflow ridges have still to fuse mutually, and with the aortopulmonary septum. Hence, a narrow aortopulmonary foramen is still present distally between the subpulmonary and subaortic channels. The connections of the subaortic and subpulmonary channels with the ascending aorta and pulmonary trunk, respectively, now occupy left and right positions (Supplemental Figure 14; [67,129,137]). This increasingly spiraling course of the intrapericardial arterial trunks corresponds in time with the unwinding of the spiraling course of the muscular outflow tract and its endocardial ridges [138] (Figures 8 and 10). The still short swellings, which guard the narrow lumen of the developing arterial valves laterally, follow the unwinding course of the main endocardial ridges. Meanwhile, the distal part of the endocardial ridges of the outflow tract begins to increase in diameter relative to the proximal counterparts. This increase in size presages the remodeling of their distal surfaces into the arterial valvar leaflets during the next 2 stages (Figure 8, upper panel). The carotid ducts have narrowed further. The artery of the right 6th arch is now narrower than the left one, in particular just distal to the origin of the right pulmonary artery. The diameter and perfusion of the left-sided dorsal aorta further increase [139].

Carnegie stage 17. At this stage, ~40 days have passed since fertilization [13]. The reconstructed specimen is shown in Supplemental Figure 10. Compared to preceding stages, limited changes were noted in the arrangement of the systemic venous sinus. The superior and inferior atrioventricular cushions have fused, along with the cap on the leading edge of the primary atrial septum, thus closing the primary atrial foramen (Figure 5; [11]). This site of fusion is reinforced on its right side by the dorsal mesenchymal protrusion, or vestibular spine. Simultaneously, a wide secondary foramen forms due to the breakdown of the dorsal portion of the primary atrial septum. Myocardium surrounds the stem of the pulmonary vein, which from this stage onwards begins to expand radially, suggesting an increase in blood flow (Figure 11). Small lateral cushions have appeared in the left and right margins of the atrioventricular canal.

The well-developed trabeculations of left and right ventricles form a complex 3-dimensional network [56], and have developed extensive gap-junctional contacts [140,141] and myofibers [142]. These properties reflect their faster conduction and stronger contraction [143,144]. The appearance of a compact left ventricular myocardial wall shows that multiplication of cardiomyocytes at the epicardial side of the ventricular walls now exceeds that in the inner trabecular layer [5]. The compact myocardium does not arise, as is often suggested, by condensation of the trabecular network [145]. While the muscular ventricular septum develops equally from right- and left-ventricular contributions during the phase of trabecular growth, the contribution of cardiomyocytes now becomes proportional to growth in the compact ventricular walls [87]. The peri-tricuspid part of the interventricular foramen, encircling the right atrioventricular orifice, continues to expand in a rightward direction, while its subaortic part remains bordered cranially by the inner curvature and caudally by the crest of the muscular ventricular septum (Figure 6).

In terms of volume, the myocardium of the middle portion of the outflow tract does not grow noticeably between CS15 and CS20 [48,146]. In overall architecture, nonetheless, it undergoes an impressive change in appearance. Its length decreases abruptly to <50% of its original length in the ~2 days separating CS16 from CS17 (Figure 7, left-sided graph; [147]). Much of the effective shortening can be attributed to it changing from a long tubular configuration at CS16 to a shorter figure-of-eight configuration at CS17 (Figure 7, lower panel). The waist of the figure-of-eight corresponds with the developing medial walls of the subpulmonary and subaortic channels. In addition, the proximal portion of the outflow tract itself becomes

progressively more wedge-shaped, with its greatest length along the subpulmonary channel and its shortest length along the subaortic channel. The proximal portion of the outflow tract of birds undergoes an almost identical change in appearance at a comparable stage of development [148]. The changing shape of the proximal outflow tract is the prelude of its incorporation as the smooth-walled infundibulum into the right ventricle, and as the aortic vestibule into the left ventricle in the next stages [83,84,106,147].

The aortopulmonary septum [149] has fused with the septal and parietal ridges. The fusion of the endocardial ridges mutually now has passed through the middle portion of the outflow tract. As a result, the neural-crest cells of the aortopulmonary septum and the prongs become sequestered inside the ridges as a dense central "whorl" of cells between the anlagen of the arterial valves (Figures 8, lower panel, and 9, upper panel). The developing aortic and pulmonary roots themselves occupy right-caudal and left-cranial positions, respectively (Figure 9, lower panel), which represents their definitive position (Figure 10, graph). The distal parts of the septal and parietal ridges undergo a similar change in shape as the corresponding part of the myocardial outflow tract. They now resemble heart-shaped structures with wide downstream "ears" separated by median furrows that presage their separation and allocation to the left and right semilunar leaflets of the aortic and pulmonary roots, respectively (Figure 8, upper panel). The lateral swellings have also increased markedly in size at this stage (Figure 9, upper panel). Concomitantly with the distal widening of the ridges and swellings, there is movement in their position relative to the distal orifices of the subaortic and subpulmonary channels (Figure 10, graph). The ridges in the proximal outflow tract have still to fuse.

Since the myocardium of the middle part of the outflow tract hardly proliferates [48,146], and the addition of new cardiomyocytes from the second heart field has ceased, the fishmouth has lost its characteristic appearance. The non-myocardial cells that continue to populate the distal outflow tract, now interpose between the distal margin of the myocardial walls and the pericardial reflection. Consequently, the myocardial boundary moves away from the pericardial reflection.

Concomitant with the marked reduction in length of the myocardial outflow tract, the pulmonary trunk ceases to grow. The ascending aorta, in contrast, continues to increase in length well beyond CS23 (Figure 7, right-sided graph). The inner layer of the smooth muscular

wall of both arterial trunks derives from the neural crest, and the outer layer from the second heart field. The wall of the ascending aorta is mainly derived from the neural crest [115,131,150], whereas the wall of the pulmonary trunk originates predominantly in the second heart field [115,116,118,151]. These different contributions may well explain the different growth characteristics of the vessels. The epicardium that covers the intrapericardial arterial trunks expresses the morphological and molecular features of the nearby pericardium. It consists of a sheet of densely packed cuboidal cells rather than of squamous cells, which characterize the epicardium. It also expresses genes that characterize the pericardium [152-154]. This "arterial" epicardium seems to form locally, since it spreads across the arterial pole even after the removal of the pro-epicardial body [155]. Collectively, these data indicate that the arterial pole of the heart derives from the ventral wall of the pharynx, with the non-myocardial tissues entering the walls of the distal part of the intrapericardial outflow tract to form its arterial component.

Extensive changes have occurred at the arterial pole. Both dorsal aortas are still present, but the left and right carotid ducts have disappeared. Marked narrowing is now seen in the diameter of the right-sided dorsal aorta between the take-off of the 7th cervical segmental artery and its confluence with the left-sided dorsal aorta, while the lumen of the artery of the right 6th arch has all but obliterated distal to the origin of the right pulmonary artery.

Carnegie stage 18. At this stage, ~43 days have passed since fertilization [13]. The reconstructed specimen is shown in Supplemental Figure 11. Compared to the previous stage, the venous part of the heart has only changed to a limited extent. Pectinate muscles, first identifiable as small stubs of the inner myocardial layer at CS14, now begin to expand in both appendages. The primary atrial septum and the secondary foramen remain comparable to the previous stage (Figure 5). Cardiomyocytes are now populating the dorsal mesenchymal protrusion, or vestibular spine, and the mesenchymal cap to form the well-developed ventro-caudal muscular rim of the atrial septum [133]. The diameter of the pulmonary veins has increased further (Figure 11, graph). Reflecting atrial growth, the myocardial atrioventricular canal changes in appearance from tubular to funnel-shaped, becoming transformed into the vestibules of the atrioventricular valves. The position and relative size of both lateral endocardial cushions in the canal do not change.

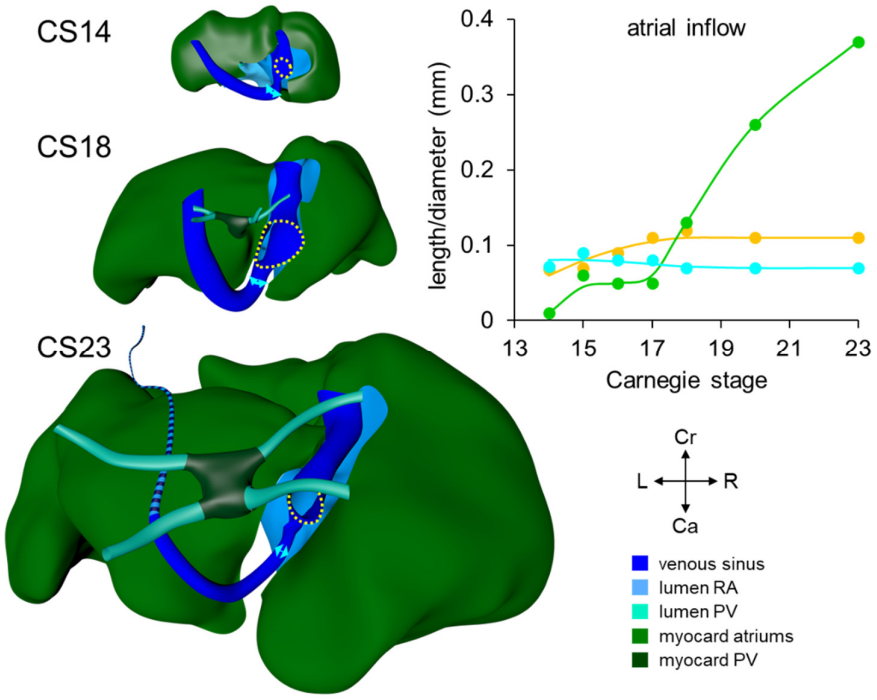

Figure 11. Pictorial timeline of the developing pulmonary veins and coronary sinus. The pulmonary vein acquires a lumen at CS14, while its stem begins to myocardialize at CS18. After the initial increase in diameter of the pulmonary vein (green symbols in graph), which reflects the appearance of its lumen, the diameter hardly changes up to CS17. Thereafter, the diameter of the pulmonary stem rapidly increases, whereas the axial length up to its first bifurcation remains constant (orange symbols). This growth pattern presages the absorption of the myocardialized part of the pulmonary vein in the wall the left atrium. Between CS14 and CS23, the diameter of the left sinus horn near its confluence with the right sinus horn remains constant (cyan symbols in graph, and double-headed arrows in left-sided images), implying a gradual decrease in blood flow. Between CS21 and CS22, the distal portion of the left sinus horn and left superior caval vein shrink more rapidly and become the ligament of Marshall (hatched blue coding), while the proximal portion of the sinus horn becomes the coronary sinus. The yellow dashed ring marks the position of the inferior caval vein. All images are also available as preset views in the corresponding 3D-PDFs.

While the structural components that are responsible for ventricular septation become morphologically identifiable, the right ventricle gradually begins to occupy a more cranial position relative to the left ventricle (Figure 4). The junction of the left ventricular inlet and outlet, with the latter still represented by the peri-subaortic component of the interventricular foramen, is guarded mainly by the superior endocardial cushion (Figure 5). The lesser curvature, forming the cranial margin of the foramen, is still muscular. The junction between the right ventricular inlet, known as the tricuspid gully [135], and the outlet is formed by the fusing superior and right-lateral endocardial cushions. By this stage, only a small connection, representing the middle part of the original interventricular foramen and also known as the tertiary interventricular foramen [156], remains between the cavity of the right ventricle and that

of the root of the subaortic outflow tract. This middle part of the interventricular foramen is bounded ventromedially by the muscular ventricular septum, dorsolaterally by the fused proximal ridges of the outflow tract, and dorsally by the fusing rightward margins of the atrioventricular cushions (Figures 5 and 6, and next paragraph). The location of the borders of the right ventricular (tricuspid) inlet and left ventricular (subaortic) outlet parts of the original interventricular foramen can still be visualized by the shape of the GlN ring (Figure 6). Because its subaortic portion no longer expresses the epitope, we have assumed its position to be in the inner curvature, where it is found in embryonic chickens [136,157]. The GlN-positive tissue in the septal structures identifies the location of the atrioventricular conduction system [88,158]. In contrast to the relatively narrow atrioventricular junctions, the junctions between the ventricles and the bases of the subaortic and subpulmonary parts of the outflow tract are wide. The subaortic component of the proximal outflow tract, however, still remains positioned above the cavity of the right ventricle, but its cavity is now contiguous with that of the left ventricular outlet. This remodeling provides the left ventricle with unhindered vascular access to the subaortic outflow channel, thus allowing closure of the middle portion of the interventricular foramen to proceed, with closure completed at CS20.

The wedge shape of the myocardial component of the outflow tract, with its blunt side over the outer curvature, and the sharp edge in the inner curvature, becomes more pronounced. The septal and parietal endocardial ridges have now fused across their entire length (Figures 9 and 10, lower panels). The distal-to-proximal fusion of the ridges occurs exclusively in the endothelium overlying the prongs of neural crest cells. The site of fusion is, therefore, marked by the dense central whorl of neural crest cells (Figure 8, lower panel and Figure 9, upper panel). The whorl subsequently disintegrates rapidly due to apoptosis [125,159-161], but some neural crest cells persist in the semilunar valves [113,162], with other remnants sometimes persisting as the so-called conus tendon [163,164]. The temporary prominence of the neural crest may explain why its ablation interferes with septation of the outflow tract [125]. Proximally, cardiomyocytes originating in the adjacent ventricular walls are invading the remaining mesenchymal shell of the fused ridges, thus forming a dumbbell-shaped muscular wall between the subaortic and subpulmonary channels (Figure 8, lower panel; [125]). The myocardializing area is continuous on its medial side with the crest of the muscular ventricular septum and on its lateral side with the parietal wall of the myocardial outflow tract (118). This myocardialization occurs in mammals [135,165] and birds [148]. It progresses from proximal to distal, in other words, opposite to the direction of septation.

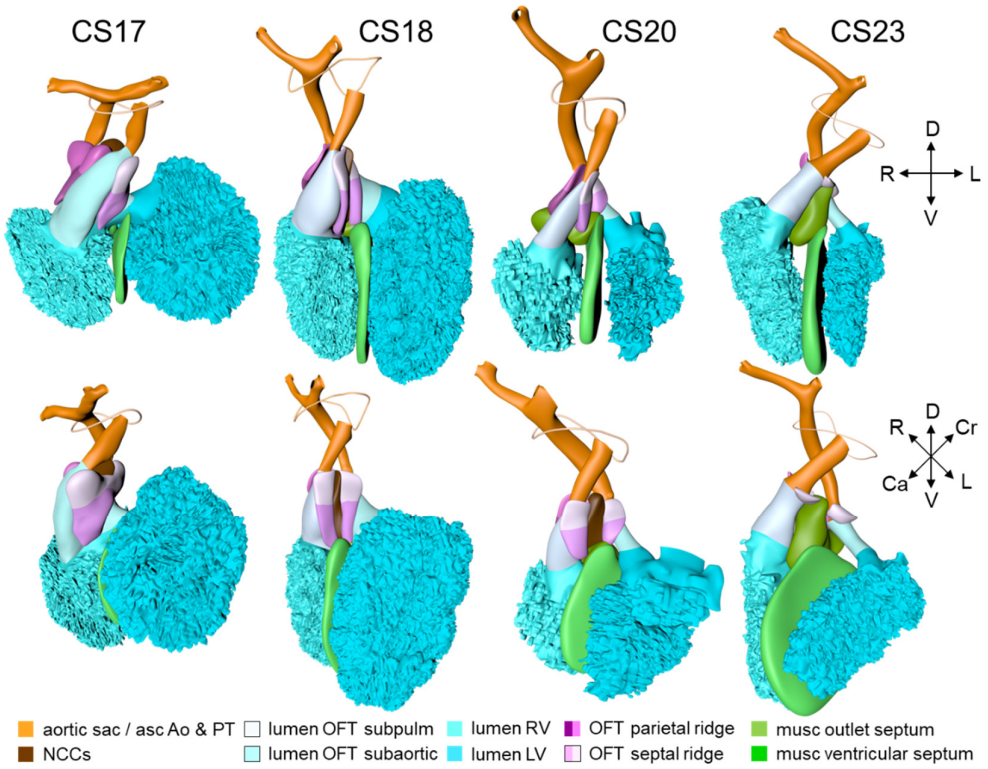

Figure 12: Pictorial timeline of the formation of the subpulmonary infundibulum. The upper panel shows cranial views of the lumens of the left and right ventricles, the muscular ventricular septum, the lumen of the outflow tract with ridges and neural crest, and the arterial trunks, while the lower panel shows left lateral views of the same structures. On completion of the fusion of the proximal outflow tract ridges at CS18, the neural crest cells disappear and myocardialization begins (Figure 8, lower panel). Myocardialization proceeds from proximal to distal, opposite to the direction of septation, reaching the arterial valves at CS23. The myocardial septum, which then separates the subpulmonary and subaortic channels, also known as the embryonic outlet septum, is located on the right side of the muscular ventricular septum and is topographically part of the right ventricle. This right-sided position accounts for subsequent development into the free-standing muscular infundibulum. At CS23, the base of the subaortic channels is on the left side of the muscular ventricular septum, but the aortic root has not yet been incorporated in to the base of the left ventricle. All images are also available as preset views in the corresponding 3D-PDFs.

Cup-shaped arterial valvar leaflets have formed in the distal part of the muscular outflow tract. The myocardial support provided to the still plump leaflets of the arterial valves may assist their closure. Growth of the myocardium in the distal outflow tract, however, slows further subsequent to formation of the arterial roots [146]. The position of the arterial valves was previously put at the dog-leg bend [8,106,166]. In reality, the arterial roots, containing the semilunar valvar leaflets, have significant length, and derive from the entire middle portion of the outflow tract. Their proximal boundary corresponds roughly with the dog-leg bend, which is present between the two parts of the myocardial outflow tract until CS16. At CS18, this boundary is

847 marked by the transition of the thin layer of myocardium that surrounds the middle outflow
848 tract into the much thicker myocardium of the proximal outflow tract. Their distal boundary,
849 the sinutubular junction, corresponds with the distal end of the endocardial ridges (Figures 7,
850 lower panel and Figure 8, upper panel). The coronary arteries originate from an endothelial
851 outgrowth of the aortic base [167,168]. The stem of the left coronary artery is first seen at CS18,
852 whereas that of the right coronary artery forms 2-3 days later at CS19 [169-173]. These coronary
853 stems contact a periaortic vascular plexus which, in turn, contacts the ventricular coronary
854 plexus [168]. The main coronary trunks can be located in the relatively thick epicardial areas in
855 the atrioventricular and interventricular grooves.

856 Distally, the arteries within the pharyngeal arches, along with the dorsal aortas, become
857 increasingly asymmetric in distribution, with regression mostly seen on the right side. The
858 artery of the right 6th arch has disappeared between the origin of the right pulmonary artery and
859 the dorsal aorta. The right pulmonary artery, therefore, appears to arise directly from the
860 pulmonary trunk. The right dorsal aorta itself tapers off between the origin of the 7th segmental
861 artery and the confluence of both dorsal aortas, subsequently disappearing at CS20. Meanwhile,
862 the walls of the large arteries become progressively better organized, which reflects increased
863 expression of extracellular matrix proteins in this period [174].

864 **Carnegie stage 20.** For stages 19 through 23, Streeter changed his staging system from one
865 based on qualitative morphological criteria to one based on a more quantitative assessment of
866 organ development [175]. With fewer features changed qualitatively, we have reconstructed only
867 2 stages. Stage 20 is reached when ~49 days have passed since fertilization [13]. The
868 reconstructed specimen is shown in Supplemental Figure 12. Compared to CS18, only limited
869 differences in the venous part of the heart are seen. The caudal part of the left cardinal, or
870 hemiazygos, vein has disappeared [69]. The atrial appendages have become prominent
871 cranioventral extensions, with the appendages still being similar in size. The stem of the
872 pulmonary veins has further increased in diameter (Figure 11, graph), with its first division
873 now having acquired a myocardial wall. The myocardial atrioventricular canal still resembles
874 a very shallow funnel, in which superior and inferior atrioventricular cushions are no longer
875 separately distinguishable [176]. Hence, they are depicted as hatched in the reconstruction. The
876 left ventricle has now acquired a thick compact myocardial wall and, concomitantly, a

pronounced ventrally pointing apex, while the thinner-walled right ventricle has mainly enlarged radially, extending more forward or cranially than the left ventricle (Figure 4).

The middle part of the tripartite interventricular foramen, which was located between the crest of the muscular ventricular septum, the rightward margins of the atrioventricular cushions, and the myocardializing ventricular end of the parietal outflow ridge [127], has now closed (Figure 5). Closure is brought about by extension of the right-sided margins of the endocardial cushions towards the muscularizing proximal outflow ridges [8,156,177]. The newly formed septum does not myocardialize. It is known, therefore, as the membranous ventricular septum [8,156,178]. The position of the GlN ring identifies the borders of the two persisting parts of the initial interventricular foramen (Figure 6). Of these, the right atrioventricular junction now occupies a near-frontal plane between the ventricular septal crest medially and the atrioventricular junction laterally, while the left ventricular outlet and the subaortic channel follow a more oblique course between the crest of the ventricular septum and the inner curvature of the heart. Myocardialization of the fused proximal ridges has progressed further distally towards the arterial roots (Figures 8, lower panel, and 12). The valvar leaflets have become longer and thinner, with the aortic and pulmonary parts separated by the remaining distal part of the neural-crest whorl. The arterial walls of the valvar sinuses are beginning to form. The left and right semilunar leaflets of both arterial valves remain within the persisting collar of outflow tract myocardium. Distal to the developing sinutubular junction, the walls of the ascending aorta and pulmonary trunk have an arterial phenotype. The right-sided dorsal aorta, which was still identifiable as a rudimentary vessel at CS19, has disappeared at CS20.

Carnegie stage 23. At this last Carnegie stage, ~56 days have elapsed since fertilization [13]. The reconstructed specimen is shown in Supplemental Figure 13. Between CS14 and CS23 the diameter of the left sinus horn does not change (Figure 11, graph), implying that it receives an increasingly smaller percentage of the systemic venous blood. Accordingly, the left cardinal vein starts to attenuate between the junction of the left subclavian and jugular veins cranially, and its passage in the left atrial ridge between the left inferior pulmonary vein and the left atrial appendage caudally. Meanwhile, the brachiocephalic vein is forming from merging venous spaces that arise between both jugular veins just cranial to the aortic arch. Remodeling occurs between CS20 and CS21, with only a minute left common cardinal vein present at CS22, the lumen of which has disappeared at CS23 [11]. The distal obliterated part of the left sinus horn is

known as the ligament of Marshall [179,180], whereas the remaining proximal part is known as the coronary sinus. The atrial appendages have increased further in size, and their pectinate muscles are well developed. Myocardium now surrounds the pulmonary veins up to their second division. The diameter of the stem of the pulmonary veins continues to increase (Figure 11, graph), preluding the incorporation of the pulmonary veins as 2 separate tributaries into the roof of the left atrium in the 9th week of development and as 4 tributaries in the 14th week [53]. A fold now begins to form in the roof of the right atrium just rightward of the primary atrial septum (Figure 5; [133]). It is against this fold, which is incorrectly known as the secondary atrial "septum", that the primary septum will eventually rest to close the oval foramen.

By now, the leaflets of the atrioventricular valves are forming, although tendinous cords have yet to develop. The leaflets, furthermore, still contain myocardium on their ventricular surface [181]. Fragmentation of the myocardial floor of the tricuspid gully gives atrial blood access to the right ventricular cavity via conduits that pass the septomarginal trabeculation cranially (pre-existing) and caudally (newly formed) [135]. In both ventricles, the papillary muscles begin to form by consolidation of aggregating trabeculations, with the compaction starting at the valve leaflets and moving in the direction of the compact ventricular walls. Epicardially-derived cells have begun to induce insulation within the atrioventricular junctions, and have populated the lateral cushions [91,182]. During CS21 and CS22, the whorl of neural crest cells in the ridges of the proximal outflow tract all but disappears, while myocardialization continues. As already explained, the so-called tendon of the conus, a cord-like band between the aortic and pulmonary roots [163,164], is an inconsistent distal remnant of the whorl. The still long subaortic outlet now passes between the developing mitral valve, the muscular ventricular septum, and the muscularized septum in the proximal outflow tract. The subpulmonary outlet passes between the muscularized septum in the proximal outflow tract and the free right ventricular wall.

The muscular septum in the proximal outflow tract, also known as outlet septum, is normally a temporary embryological structure. It changes in shape and orientation from a dumbbell-like structure perpendicular to the muscular ventricular septum at CS20 to a flat blade almost parallel to the muscular ventricular septum at CS23 (Figure 12). Extension of its myocardialization towards the developing arterial roots underlies this change in orientation. This positional change coincides with the incorporation of the proximal outflow tract into the ventricles [83,147,148], and transforms the transitory outlet septum into the smooth medial wall of the right ventricle, the dorsocranial part of which becomes the "free-standing" muscular

subpulmonary infundibulum [163]. The attribution of the muscular septum of the outflow tract as a mostly right-ventricular structure [127] can be best appreciated if the ventricular cavities, muscular septum, and (sub-)aortic and (sub-)pulmonary channels are observed from the left (Figure 12, lower panel). The developmental events underlying the transformation of the embryonic outlet septum from a septal to a mural structure are still poorly understood, but probably reflect the asymmetric growth of the increasingly wedge-shaped and transversely oriented right ventricle (Figure 4). Should the middle portion of the interventricular foramen fail to close, then the result will be a perimembranous ventricular septal defect. Should the asymmetric growth of the right ventricle and the transfer of the aortic root to the left ventricle be hampered, however, the result will be tetralogy of Fallot, or double-outlet right ventricle. In all these settings, it remains possible to recognize a muscular or fibrous outlet septum [183].

Between CS18 and CS23, the arterial valvar leaflets become slenderer, the walls of the sinuses better formed, and the ventriculoarterial and sinutubular junctions identifiable structures. As development progresses, the myocardial cells of the valvar cuff covering the left and right leaflets do not proliferate, but become diluted in the proliferating epicardial connective tissues. Remnants of this myocardium can, nevertheless, persist at least until the 3rd trimester (our unpublished observations) and perhaps into adult life.

Coda

We have described the morphological development of the human heart between its first appearance at CS9 up to CS23, when almost all structures of the definitive heart have formed, although at this stage several have still to reach their relative sizes and definitive positions. Because we used embryos that had been carefully staged at the Carnegie Institution without exclusive attention to heart development, we were able to assign critical events in heart development to specific stages of human embryonic development.

The first heart field produces the embryonic left ventricle, which contributes eventually to no more than parts of the definitive left ventricle to the formed heart [16,19,20]. Ongoing addition of cardiomyocytes from the second heart field to the venous and arterial poles of the embryonic left ventricle, and differentiation into cardiac compartments, is therefore necessary to form the definitive heart [24,48,111]. Accordingly, the atriums form at CS10-11, and the systemic venous

970 sinus at CS12. The embryonic right ventricle forms at CS10, while the myocardial outflow
971 tract forms at CS11-12. The pharyngeal arch arteries are successively added between CS12 and
972 CS14, and the non-myocardial distal portion of the outflow tract begins to appear at CS15.
973 Furthermore, endocardial cushions and ridges form at CS14 to allow for separate blood flows.
974 Development progresses, therefore, by addition of cardiomyocytes at the venous and arterial
975 periphery of the heart tube (Table 1). This "peripheral growth" model of heart development
976 ends when the building plan of the heart has been established at the phylotypic stage (CS13).
977 Subsequently, central structures in the heart, such as the atrioventricular canal, inner heart
978 curvature, and muscular outflow tract temporarily retain their relatively undifferentiated status
979 as remnants of the primary heart tube. They contribute to the internal remodeling that is
980 necessary to achieve septation [108]. Septation is associated temporally with the appearance of
981 the arterial trunks in the distal portion of the outflow tract, but it is not known, to our
982 knowledge, whether the achievement of separate pulmonary and systemic circulations is
983 associated with a new functional capacity. Since the timing corresponds with the transition of
984 the yolk-sac to the (hemo-)chorial placenta [101,184], we submit that the enhanced pumping
985 efficiency or capacity is a determining factor.

986 The description of the respective developmental stages required an unexpected difference in
987 the number of words needed to delineate stage-specific differences. On average, 500-800 words
988 sufficed to describe the incremental changes in heart development for most stages, but the
989 description of CS14 and CS(17+18) required double that number. Human CS13 or "Horizon
990 XIII" [175] embryos have developed 30-36 somites [185], which makes them comparable to Theiler
991 stage 16 mouse embryos [186]. This stage is considered "phylotypic" because the basic body plan
992 of vertebrate embryos has been established at this stage and gene-expression profiles between
993 model species of vertebrate groups are most similar [15]. Subsequent to this very conserved stage,
994 CS14 is characterized by the appearance of an array of new features, such as the venous valves,
995 the primary atrial septum, a patent pulmonary vein, the muscular ventricular septum, the ridges
996 in the outflow tract, the cardiac neural crest, the non-myocardial walls of the distal outflow
997 tract, the beginning transformation of the aortic sac into the arterial trunks, and the appearance
998 of the last and special pair of pharyngeal arch arteries [109]. The transition of CS13 to CS14 does
999 not, of course, proceed abruptly, but should be considered as a change in developmental pace.

The reverse is seen at CS18, at which stage marsupial embryos have advanced sufficiently to survive outside the womb even though, for instance, the interventricular foramen has yet to close [187]. Perhaps to prepare for extrauterine survival marsupials or for perfusion of the (hemo-)chorial placenta in eutherian mammals, the heart extensively remodels during CS17 and CS18. It is at these stages that fusion occurs between the superior and inferior atrioventricular cushions, and between the septal and parietal ridges of the outflow tract. During the same period, the interventricular foramen remodels to accommodate unimpeded systemic and pulmonary blood flows, the mesenchymal components of the atrial septum and the outlet septum myocardialize to buttress the structures to which they contribute, the coronary arteries form to nourish the newly formed compact wall of the ventricles, the muscular outflow tract remodels with incorporation of its proximal part into the ventricles, and a start is made with the development of valves. It is closure of the middle part of the interventricular foramen by formation of the membranous septum at CS20 that completes septation. Based on these features, we hypothesize that embryonic heart development includes an early phase, during which its basic building plan is laid down, in accordance with the peripheral growth model. There is then a later phase during which the heart remodels to cope with the requirements of postnatal or placental circulation in marsupial and eutherian mammals, respectively [101,184]. The subsequent fetal phase varies markedly in length between species. It can, in the case of marsupials, even be non-existent, with development proceeding in a pouch, which is outside the womb.

Quantitative morphology

We have taken great care to calibrate the scale cubes that we added to each of the reconstructions. Because of this, they permit comparisons of structures between stages in real size. They can be used to settle arguments of the effects of differential growth on shape. Especially in cardiac structures with components that differ greatly in growth rate, such as the respective parts of the outflow tract, such proportional comparisons are useful. Accordingly, the distal myocardial component of the outflow tract was found hardly to increase in size after CS14, whereas the myocardium of the proximal outflow tract continues to contribute quantitatively after its remodeling into the infundibulum of the right ventricle (Figures 7, lower panel, and 8, upper panel). Such comparisons further show that the formation of the semilunar leaflets of the arterial valves started with a selective increase in the diameter of the distal

endocardial ridges at CS16, the forming of a dividing furrow at CS17, and the division into aortic and pulmonary roots at CS18. These pictorial timelines further revealed that the absence of growth in the distal myocardial outflow tract was compensated for by growth of the intrapericardial arterial trunks, in particular the aortic trunk (Figure 7, right graph). Such comparisons, therefore, allow a coherent account to be advanced regarding the development of the arterial pole of the heart.

Attention to the segmental structures, such as the somites and spinal ganglia, and longitudinal structures, like the dorsal aorta, gut, and central nervous system, in the reconstructions were instrumental in determining changes in the relative positions of organ structures. In particular developmental changes in the helical course of the wall of the heart tube, parts of which have been controversial for a long time, could be measured accurately. During the looping phase of heart development (CS10-CS12), the helical course of the wall was clockwise in direction when following the bloodstream (Figure 3). Following this pre-pattern, the endocardial ridges of the outflow tract, which made their appearance at CS14, spiraled clockwise. During the next 3 stages (~1 week), this spiraling course was reversed [137,138], becoming transferred to the intrapericardial arterial trunks (Figure 10, graph), in other words to non-myocardial structures. This unwinding precedes the extensive remodeling of the myocardial outflow tract between CS16 and CS18, but whether there is a relation between these structures remains to be established.

Limitations of the study

We have provided 12 detailed reconstructions of human embryonic hearts between CS9 and CS23. Although it can reasonably be stated that 12 models cannot visualize all of cardiac development, we were able to provide a continuous account of the changes in size and shape of the heart. We did not encounter major gaps in our description of the models. A valid question, nevertheless, is whether we have accounted for all variation. Although the answer is obviously “no”, differences between specimens could usually be explained as small differences in degree of individual development rather than deviation from the expected morphology. An example is the CS9 model in our series. This embryo (Carnegie #3709) has 4 or 5 somites, which places it in the least advanced CS10 group, but its cardiovascular development is least developed in the entire series described by Davis [14]. Questions can, therefore, be posed with

regard to the normality of this embryo. Since two additional embryos with 5 formed somites show a near identical morphology with respect to its cardiovascular system [9,24], we assume that the reconstruction represents a normal stage of heart development. Our findings in human embryos fall in line with earlier observations in mice, revealing that heart and early somite development do not proceed strictly synchronously [43,188]. Another example is the appearance of the pulmonary arteries in our model embryo at CS15, whereas Sizarov and colleagues associated their appearance with CS14 [39]. In the Carnegie collection, the pulmonary arteries make their appearance in ~75% of the 44 embryos at CS14 and in the remainder at CS15 [11]. Such data indicate that small interindividual differences exist in the developmental timing of organogenesis. The most important limitation of the present series is probably that the models still contain mistakes. Because the models are made in the software program Cinema4D, such mistakes can be corrected relatively easily. We, therefore, encourage readers to report such errors.

Materials and methods

Embryos

This study was undertaken in accordance with the Dutch regulations for the proper use of human tissue for medical research purposes. Staged human embryos were obtained from the Digitally Reproduced Embryonic Morphology (DREM) project (Dr John Cork; Cell Biology & Anatomy, LSU Health Sciences Center, New Orleans; https://www.ehd.org/virtual-human-embryo/about.php, http://virtualhumanembryo.lsuhsc.edu). These embryos are part of the Carnegie collection, Washington D.C., USA. We reconstructed 12 hearts from human embryos obtained between ~26 and ~56 days of development subsequent to fertilization. In addition to the reconstructed and modelled embryos, we also studied the immunohistochemically stained sections of human embryonic hearts collected and produced by Viragh and Wessels [88,107,189], Sizarov [24,39,122,132,190], and Ya [24]. We used the criteria of O'Rahilly, as modified in 2010 [13], to correlate Carnegie stages of human development with days of development subsequent to fertilization. The description of developmental processes in human embryos is, where appropriate, underscored with experimental data from other mammals, in particular mice, and if fitting, also with data from chickens. Theiler's staging system [186] was used to correlate the stages in murine development with the Carnegie stages, while appendix I of Kirby's

monograph on cardiac development [191] was used to correlate Hamilton and Hamburger's staging system of chicken embryos [192] to the Carnegie stages (Supplemental Figure 1). Heart development in chicken embryos was carefully tabulated by Martinsen [193], but this study does not systematically correlate chicken to mammalian development. Segmental levels in the embryo were determined perpendicular to the curvature of the spinal cord. Segmental levels were related to somite number up to CS13, and to spinal ganglion number from CS14 onwards. Because the occipital somites do not induce spinal ganglia, the latter number is 4 units smaller.

Image acquisition, 3D-reconstruction and visualization

Processing of the digital images, and calculation of voxel size, were performed as described previously [69]. AMIRA (version 2019.3; FEI Visualization Sciences Group Europe, Merignac Cedex, France) was used to generate 3D reconstructions. Preliminary alignment of consecutive sections was performed automatically with the least-squares method, followed by further manual alignment. The definitive alignment also accounted for curvatures in the sagittal and transverse planes of the body axis of the embryo. Existing images of the embryo before sectioning or age-matched embryos that were imaged with magnetic resonance were used as the template for proper alignment (e.g. http://embryo.soad.umich.edu, https://www.prenatalorigins.org/virtual-human-embryo, http://virtualhumanembryo.lsuhsc.edu). Delineation of heart structures was performed manually, using the immunohistochemically stained sections described elsewhere [24,39,88,107,122,132,189,190] as guides.

Polygon meshes from all reconstructed materials were exported via 'vrml export' to the remodeling software Cinema 4D (version R21; MAXON Computer GmbH, Friedrichsdorf, Germany). The accuracy of the remodeling process was safeguarded by simultaneous visualization in Cinema 4D of the original output from Amira and the remodeled Cinema model. Subsequently, the Cinema 3D-model was exported via 'wrl export' to Adobe's portable device format (PDF) reader version 9 (http://www.adobe.com) for the generation of 3D-interactive PDF files (Supplemental Figures 2-13). The reader is encouraged simultaneously to read the text and inspect the corresponding interactive PDFs. This is because their rotational options ("live" images) allow a much better understanding of the complex local topography than do "still" images and text.

Measurements

For all goniometric measurements, the structures of interest were aligned using long craniocaudal structures, such as the dorsal aorta or neural tube. All axial lengths were measured in the Cinema reconstructions with the "spline" function, which takes the curvature of structures into account. Dots in the graphs represent measured values, while the lines connecting the observed values were constructed manually.

Description

The descriptions of the embryonic hearts follow the sequential segmental approach [194]. We use cranial-caudal, dorsal-ventral, and left-right to describe topographical relations, with the cervical and upper thoracic vertebral column being dorsal. The terms proximal and distal refer to positions relative to the center of the heart.

Acknowledgements

We thank Dr. John Cork (New Orleans) for making extra sections of embryos included in the DREM collection available and Dr Antoon Moorman (Amsterdam) for constructive discussions and comments. Furthermore, we would like to thank our bachelor students, who worked on heart development as part of their academic internship. The financial support of 'Stichting Rijp' is gratefully acknowledged.

Author contributions

J.P.J.M.H. was responsible for data collection, analysis and visualization. N.K., S.E.K., and W.H.L. participated in data analysis and interpretation. J.P.J.M.H., N.K., and G.M.C.M. were responsible for the reconstruction and modeling of the 3D-PDFs. S.E.K and R.H.A. participated in data analysis and interpretation, provided guidance, and edited the manuscript. J.P.J.M.H. and W.H.L. conceived the study and wrote the manuscript.

Competing interests

The authors declare no competing interests.

References

1 Born, G. Die Plattenmodelliermethode. *Archiv f. mikroskopische Anatomie* **XXII**, 584-599 (1883).

2 Hopwood, N. *Embryos in wax: models from the Ziegler studio*. (2002).

3 Blechschmidt, E. Rekonstruktionsverfahren mit Verwendung von Kunststoffen. Ein Verfahren zur Ermittlung und Demonstration von Entwicklungsbewegungen. *Z Anat Entwicklungsgesch* **118**, 170-174 (1954).

4 Blechschmidt, E. *Der menschliche Embryo*. (Friedrich-Karl Schattauer-Verlag, 1963).

5 Van Mierop, L. H., Alley, R. D., Kausel, H. W. & Stranahan, A. Pathogenesis of transposition complexes. I. Embryology of the ventricles and great arteries. *Am J Cardiol* **12**, 216-225 (1963).

6 Netter, F. H. & van Mierop, L. H. S. *Embryology, in: F.H. Netter. The CIBA collection of medical illustrations*. Vol. 5, section III 111-130 (Hennegan Co, 1992).

7 de Vries, P. A. & de Cusance Morant Saunders, J. B. Development of the ventricles and spiral outflow tract in the human heart : a contribution to the development of the human heart from age group IX to age group XV. *Contributions to Embryology* **37**, 87-114 (1962).

8 Kramer, T. C. The partitioning of the truncus and conus and the formation of the membranous portion of the interventricular septum in the human heart. *Am J Anat* **71**, 343-370 (1942).

9 de Bakker, B. S. *et al.* An interactive three-dimensional digital atlas and quantitative database of human development. *Science* **354**, doi:10.1126/science.aag0053 (2016).

10 O'Rahilly, R. The timing and sequence of events in human cardiogenesis. *Acta Anat (Basel)* **79**, 70-75 (1971).

11 McBride, R. E., Moore, G. W. & Hutchins, G. M. Development of the outflow tract and closure of the interventricular septum in the normal human heart. *Am J Anat* **160**, 309-331, doi:10.1002/aja.1001600308 (1981).

12 Dhanantwari, P. *et al.* Human cardiac development in the first trimester: a high-resolution magnetic resonance imaging and episcopic fluorescence image capture atlas. *Circulation* **120**, 343-351, doi:10.1161/CIRCULATIONAHA.108.796698 (2009).

13 O'Rahilly, R. & Muller, F. Developmental stages in human embryos: revised and new measurements. *Cells Tissues Organs* **192**, 73-84, doi:10.1159/000289817 (2010).

14 Davis, C. L. Development of the human heart from its first appearance to the stage found in embryos of twenty paired somites. *Contributions to embryology, Carnegie Institution* **107**, 247-284 (1927).

15 Irie, N. & Kuratani, S. Comparative transcriptome analysis reveals vertebrate phylotypic period during organogenesis. *Nat Commun* **2**, 248, doi:10.1038/ncomms1248 (2011).

16 Lescroart, F. *et al.* Early lineage restriction in temporally distinct populations of Mesp1 progenitors during mammalian heart development. *Nat Cell Biol* **16**, 829-840, doi:10.1038/ncb3024 (2014).

17 Chabab, S. *et al.* Uncovering the number and clonal dynamics of Mesp1 progenitors during heart morphogenesis. *Cell Rep* **14**, 1-10, doi:10.1016/j.celrep.2015.12.013 (2016).

18 Saga, Y. *et al.* MesP1 is expressed in the heart precursor cells and required for the formation of a single heart tube. *Development* **126**, 3437-3447 (1999).

19 Liang, X. *et al.* HCN4 dynamically marks the first heart field and conduction system precursors. *Circ Res* **113**, 399-407, doi:10.1161/CIRCRESAHA.113.301588 (2013).

20 Aanhaanen, W. T. *et al.* The Tbx2+ primary myocardium of the atrioventricular canal forms the atrioventricular node and the base of the left ventricle. *Circ Res* **104**, 1267-1274, doi:10.1161/CIRCRESAHA.108.192450 (2009).

21 Cai, C. L. *et al.* Isl1 identifies a cardiac progenitor population that proliferates prior to differentiation and contributes a majority of cells to the heart. *Dev Cell* **5**, 877-889 (2003).

22 Lescroart, F., Mohun, T., Meilhac, S. M., Bennett, M. & Buckingham, M. Lineage tree for the venous pole of the heart: clonal analysis clarifies controversial genealogy based on genetic tracing. *Circ Res* **111**, 1313-1322, doi:10.1161/CIRCRESAHA.112.271064 (2012).

23 Mommersteeg, M. T. *et al.* The sinus venosus progenitors separate and diversify from the first and second heart fields early in development. *Cardiovasc Res* **87**, 92-101, doi:10.1093/cvr/cvq033 (2010).

24 Sizarov, A. *et al.* Formation of the building plan of the human heart: morphogenesis, growth, and differentiation. *Circulation* **123**, 1125-1135, doi:10.1161/CIRCULATIONAHA.110.980607 (2011).

25 DeRuiter, M. C., Poelmann, R. E., VanderPlas-de Vries, I., Mentink, M. M. & Gittenberger-de Groot, A. C. The development of the myocardium and endocardium in mouse embryos. Fusion of two heart tubes? *Anat Embryol (Berl)* **185**, 461-473, doi:10.1007/BF00174084 (1992).

26 Manasek, F. J. Macromolecules of the extracellular compartment of embryonic and mature hearts. *Circ Res* **38**, 331-337 (1976).

27 Wisser, J. & Dirschedl, P. Embryonic heart rate in dated human embryos. *Early Hum Dev* **37**, 107-115, doi:10.1016/0378-3782(94)90152-x (1994).

28 Nishii, K. & Shibata, Y. Mode and determination of the initial contraction stage in the mouse embryo heart. *Anat Embryol (Berl)* **211**, 95-100, doi:10.1007/s00429-005-0065-x (2006).

29 Hikspoors, J. P. J. M. *et al.* The fate of the vitelline and umbilical veins during the development of the human liver. *J Anat* **231**, 718-735, doi:10.1111/joa.12671 (2017).

30 Buckingham, M., Meilhac, S. & Zaffran, S. Building the mammalian heart from two sources of myocardial cells. *Nat Rev Genet* **6**, 826-835, doi:10.1038/nrg1710 (2005).

31 de la Cruz, M. V. *et al.* Living morphogenesis of the ventricles and congenital pathology of their component parts. *Cardiol Young* **11**, 588-600, doi:10.1017/s1047951101000932 (2001).

32 De Bono, C. *et al.* T-box genes and retinoic acid signaling regulate the segregation of arterial and venous pole progenitor cells in the murine second heart field. *Hum Mol Genet* **27**, 3747-3760, doi:10.1093/hmg/ddy266 (2018).

33 Galli, D. *et al.* Atrial myocardium derives from the posterior region of the second heart field, which acquires left-right identity as Pitx2c is expressed. *Development* **135**, 1157-1167, doi:10.1242/dev.014563 (2008).

34 Yang, Y. P. *et al.* Second heart field and the development of the outflow tract in human embryonic heart. *Dev Growth Differ* **55**, 359-367, doi:10.1111/dgd.12050 (2013).

35 Lescroart, F. *et al.* Clonal analysis reveals common lineage relationships between head muscles and second heart field derivatives in the mouse embryo. *Development* **137**, 3269-3279, doi:10.1242/dev.050674 (2010).

36 Meilhac, S. M. & Buckingham, M. E. The deployment of cell lineages that form the mammalian heart. *Nat Rev Cardiol* **15**, 705-724, doi:10.1038/s41569-018-0086-9 (2018).

37 Hiruma, T. & Hirakow, R. Formation of the pharyngeal arch arteries in the chick embryo. Observations of corrosion casts by scanning electron microscopy. *Anat Embryol (Berl)* **191**, 415-423, doi:10.1007/bf00304427 (1995).

38 Hiruma, T., Nakajima, Y. & Nakamura, H. Development of pharyngeal arch arteries in early mouse embryo. *J Anat* **201**, 15-29, doi:10.1046/j.1469-7580.2002.00071.x (2002).

39 Sizarov, A., Anderson, R. H., Christoffels, V. M. & Moorman, A. F. Three-dimensional and molecular analysis of the venous pole of the developing human heart. *Circulation* **122**, 798-807, doi:10.1161/CIRCULATIONAHA.110.953844 (2010).

40 Dominguez, J. N., Meilhac, S. M., Bland, Y. S., Buckingham, M. E. & Brown, N. A. Asymmetric fate of the posterior part of the second heart field results in unexpected left/right contributions to both poles of the heart. *Circ Res* **111**, 1323-1335, doi:10.1161/CIRCRESAHA.112.271247 (2012).

41 Mommersteeg, M. T. *et al.* Pitx2c and Nkx2-5 are required for the formation and identity of the pulmonary myocardium. *Circ Res* **101**, 902-909, doi:10.1161/CIRCRESAHA.107.161182 (2007).

42 Bayraktar, M. & Manner, J. Cardiac looping may be driven by compressive loads resulting from unequal growth of the heart and pericardial cavity. Observations on a physical simulation model. *Front Physiol* **5**, 112, doi:10.3389/fphys.2014.00112 (2014).

43 Le Garrec, J. F. *et al.* A predictive model of asymmetric morphogenesis from 3D reconstructions of mouse heart looping dynamics. *Elife* **6**, doi:10.7554/eLife.28951 (2017).

44 Biben, C. & Harvey, R. P. Homeodomain factor Nkx2-5 controls left/right asymmetric expression of bHLH gene eHand during murine heart development. *Genes Dev* **11**, 1357-1369 (1997).

45 Honda, H., Abe, T. & Fujimori, T. The chiral looping of the embryonic heart is formed by the combination of three axial asymmetries. *Biophys J* **118**, 742-752, doi:10.1016/j.bpj.2019.11.3397 (2020).

46 Chen, L., Fulcoli, F. G., Tang, S. & Baldini, A. Tbx1 regulates proliferation and differentiation of multipotent heart progenitors. *Circ Res* **105**, 842-851, doi:10.1161/CIRCRESAHA.109.200295 (2009).

47 Watanabe, Y. *et al.* Fibroblast growth factor 10 gene regulation in the second heart field by Tbx1, Nkx2-5, and Islet1 reveals a genetic switch for down-regulation in the myocardium. *Proc Natl Acad Sci U S A* **109**, 18273-18280, doi:10.1073/pnas.1215360109 (2012).

48 de Boer, B. A., van den Berg, G., de Boer, P. A., Moorman, A. F. & Ruijter, J. M. Growth of the developing mouse heart: an interactive qualitative and quantitative 3D atlas. *Dev Biol* **368**, 203-213, doi:10.1016/j.ydbio.2012.05.001 (2012).

49 Meilhac, S. M., Esner, M., Kerszberg, M., Moss, J. E. & Buckingham, M. E. Oriented clonal cell growth in the developing mouse myocardium underlies cardiac morphogenesis. *J Cell Biol* **164**, 97-109, doi:10.1083/jcb.200309160 (2004).

50 Cano, E. *et al.* Extracardiac septum transversum/proepicardial endothelial cells pattern embryonic coronary arterio-venous connections. *Proc Natl Acad Sci U S A* **113**, 656-661, doi:10.1073/pnas.1509834113 (2016).

51 Auer, J. The development of the human pulmonary vein and its major variations. *Anat Rec* **101**, 581-594 (1948).

52 Neill, C. A. Development of the pulmonary veins; with reference to the embryology of anomalies of pulmonary venous return. *Pediatrics* **18**, 880-887 (1956).

53 Webb, S., Kanani, M., Anderson, R. H., Richardson, M. K. & Brown, N. A. Development of the human pulmonary vein and its incorporation in the morphologically left atrium. *Cardiol Young* **11**, 632-642 (2001).

54 Wessels, A. *et al.* Atrial development in the human heart: an immunohistochemical study with emphasis on the role of mesenchymal tissues. *Anat Rec* **259**, 288-300 (2000).

55 Meilhac, S. M. *et al.* A retrospective clonal analysis of the myocardium reveals two phases of clonal growth in the developing mouse heart. *Development* **130**, 3877-3889 (2003).

56 Captur, G. *et al.* Morphogenesis of myocardial trabeculae in the mouse embryo. *J Anat* **229**, 314-325, doi:10.1111/joa.12465 (2016).

57 Del Monte-Nieto, G. *et al.* Control of cardiac jelly dynamics by NOTCH1 and NRG1 defines the building plan for trabeculation. *Nature* **557**, 439-445, doi:10.1038/s41586-018-0110-6 (2018).

58 Okuno, K. *et al.* Rib cage morphogenesis in the human embryo: a detailed three-dimensional analysis. *Anat Rec (Hoboken)* **302**, 2211-2223, doi:10.1002/ar.24226 (2019).

59 McFadden, D. G. *et al.* The Hand1 and Hand2 transcription factors regulate expansion of the embryonic cardiac ventricles in a gene dosage-dependent manner. *Development* **132**, 189-201, doi:10.1242/dev.01562 (2005).

60 Takeuchi, J. K. *et al.* Tbx5 specifies the left/right ventricles and ventricular septum position during cardiogenesis. *Development* **130**, 5953-5964, doi:10.1242/dev.00797 (2003).

61 Bharadwaj, K. N., Spitz, C., Shekhar, A., Yalcin, H. C. & Butcher, J. T. Computational fluid dynamics of developing avian outflow tract heart valves. *Ann Biomed Eng* **40**, 2212-2227, doi:10.1007/s10439-012-0574-8 (2012).

62 Yoshida, H., Manasek, F. & Arcilla, R. A. Intracardiac flow patterns in early embryonic life. A reexamination. *Circ Res* **53**, 363-371 (1983).

63 Meilhac, S. M., Esner, M., Kelly, R. G., Nicolas, J. F. & Buckingham, M. E. The clonal origin of myocardial cells in different regions of the embryonic mouse heart. *Dev Cell* **6**, 685-698, doi:10.1016/s1534-5807(04)00133-9 (2004).

64 Manner, J. On the form problem of embryonic heart loops, its geometrical solutions, and a new biophysical concept of cardiac looping. *Ann Anat* **195**, 312-323, doi:10.1016/j.aanat.2013.02.008 (2013).

65 Campione, M. *et al.* Pitx2 expression defines a left cardiac lineage of cells: evidence for atrial and ventricular molecular isomerism in the iv/iv mice. *Dev Biol* **231**, 252-264, doi:10.1006/dbio.2000.0133 (2001).
66 Furtado, M. B., Biben, C., Shiratori, H., Hamada, H. & Harvey, R. P. Characterization of Pitx2c expression in the mouse heart using a reporter transgene. *Dev Dyn* **240**, 195-203, doi:10.1002/dvdy.22492 (2011).
67 Bajolle, F. *et al.* Rotation of the myocardial wall of the outflow tract is implicated in the normal positioning of the great arteries. *Circ Res* **98**, 421-428, doi:10.1161/01.RES.0000202800.85341.6e (2006).
68 Webb, S., Qayyum, S. R., Anderson, R. H., Lamers, W. H. & Richardson, M. K. Septation and separation within the outflow tract of the developing heart. *J Anat* **202**, 327-342 (2003).
69 Hikspoors, J. P. J. M. *et al.* Development of the human infrahepatic inferior caval and azygos venous systems. *J Anat* **226**, 113-125, doi:10.1111/joa.12266 (2015).
70 Orts-Llorca, F., Puerta Fonolla, J. & Sobrado, J. The formation, septation and fate of the truncus arteriosus in man. *J Anat* **134**, 41-56 (1982).
71 Anderson, R. H., Webb, S., Brown, N. A., Lamers, W. & Moorman, A. Development of the heart: (3) formation of the ventricular outflow tracts, arterial valves, and intrapericardial arterial trunks. *Heart* **89**, 1110-1118 (2003).
72 Hiermeier, F. & Manner, J. Kinking and torsion can significantly improve the efficiency of valveless pumping in periodically compressed tubular conduits. Implications for understanding of the form-function relationship of embryonic heart tubes. *J Cardiovasc Dev Dis* **4**, doi:10.3390/jcdd4040019 (2017).
73 Wang, X. *et al.* Endothelium in the pharyngeal arches 3, 4 and 6 is derived from the second heart field. *Dev Biol* **421**, 108-117, doi:10.1016/j.ydbio.2016.12.010 (2017).
74 O'Rahilly, R. & Muller, F. *Developmental stages in human embryos, including a revision of Streeter's "horizons" and a survey of the Carnegie Collection*. Vol. 637 (1987).
75 Christoffels, V. M. *et al.* Formation of the venous pole of the heart from an Nkx2-5-negative precursor population requires Tbx18. *Circ Res* **98**, 1555-1563, doi:10.1161/01.RES.0000227571.84189.65 (2006).
76 de Lange, F. J. *et al.* Lineage and morphogenetic analysis of the cardiac valves. *Circ Res* **95**, 645-654, doi:10.1161/01.RES.0000141429.13560.cb (2004).
77 Wu, B. *et al.* Nfatc1 coordinates valve endocardial cell lineage development required for heart valve formation. *Circ Res* **109**, 183-192, doi:10.1161/CIRCRESAHA.111.245035 (2011).
78 Wiese, C. *et al.* Formation of the sinus node head and differentiation of sinus node myocardium are independently regulated by Tbx18 and Tbx3. *Circ Res* **104**, 388-397, doi:10.1161/CIRCRESAHA.108.187062 (2009).
79 Mommersteeg, M. T. *et al.* Two distinct pools of mesenchyme contribute to the development of the atrial septum. *Circ Res* **99**, 351-353, doi:10.1161/01.RES.0000238360.33284.a0 (2006).
80 De La Cruz, M. V., Sanchez-Gomez, C. & Palomino, M. A. The primitive cardiac regions in the straight tube heart (Stage 9) and their anatomical expression in the mature heart: An experimental study in the chick embryo. *J Anat* **165**, 121-131 (1989).
81 Mohan, R. A. *et al.* Embryonic Tbx3(+) cardiomyocytes form the mature cardiac conduction system by progressive fate restriction. *Development* **145**, doi:10.1242/dev.167361 (2018).
82 de la Cruz, M. V., Sanchez Gomez, C., Arteaga, M. M. & Arguello, C. Experimental study of the development of the truncus and the conus in the chick embryo. *J Anat* **123**, 661-686 (1977).
83 Lazzarini, R. *et al.* The proximal segment of the embryonic outflow (conus) does not participate in aortic vestibule development. *PLoS One* **13**, e0209930, doi:10.1371/journal.pone.0209930 (2018).
84 Rana, M. S. *et al.* Trabeculated right ventricular free wall in the chicken heart forms by ventricularization of the myocardium initially forming the outflow tract. *Circ Res* **100**, 1000-1007, doi:10.1161/01.RES.0000262688.14288.b8 (2007).
85 Christoffels, V. M. *et al.* Chamber formation and morphogenesis in the developing mammalian heart. *Dev Biol* **223**, 266-278, doi:10.1006/dbio.2000.9753 (2000).

86 Van Mierop, L. H. & Kutsche, L. M. Development of the ventricular septum of the heart. *Heart Vessels* **1**, 114-119 (1985).
87 Franco, D. *et al.* Left and right ventricular contributions to the formation of the interventricular septum in the mouse heart. *Dev Biol* **294**, 366-375, doi:10.1016/j.ydbio.2006.02.045 (2006).
88 Wessels, A. *et al.* Spatial distribution of "tissue-specific" antigens in the developing human heart and skeletal muscle. III. An immunohistochemical analysis of the distribution of the neural tissue antigen GlN2 in the embryonic heart; implications for the development of the atrioventricular conduction system. *Anat Rec* **232**, 97-111, doi:10.1002/ar.1092320111 (1992).
89 Chou, D. K. *et al.* Structure of sulfated glucuronyl glycolipids in the nervous system reacting with HNK-1 antibody and some IgM paraproteins in neuropathy. *J Biol Chem* **261**, 11717-11725 (1986).
90 Lamers, W. H. *et al.* New findings concerning ventricular septation in the human heart. Implications for maldevelopment. *Circulation* **86**, 1194-1205, doi:10.1161/01.cir.86.4.1194 (1992).
91 Wessels, A. *et al.* The development of the atrioventricular junction in the human heart. *Circ Res* **78**, 110-117, doi:10.1161/01.res.78.1.110 (1996).
92 Phoon, C. K., Aristizabal, O. & Turnbull, D. H. Spatial velocity profile in mouse embryonic aorta and Doppler-derived volumetric flow: a preliminary model. *Am J Physiol Heart Circ Physiol* **283**, H908-916, doi:10.1152/ajpheart.00869.2001 (2002).
93 Al-Roubaie, S., Jahnsen, E. D., Mohammed, M., Henderson-Toth, C. & Jones, E. A. Rheology of embryonic avian blood. *Am J Physiol Heart Circ Physiol* **301**, H2473-2481, doi:10.1152/ajpheart.00475.2011 (2011).
94 Yalcin, H. C., Shekhar, A., McQuinn, T. C. & Butcher, J. T. Hemodynamic patterning of the avian atrioventricular valve. *Dev Dyn* **240**, 23-35, doi:10.1002/dvdy.22512 (2011).
95 Sedmera, D., Pexieder, T., Vuillemin, M., Thompson, R. P. & Anderson, R. H. Developmental patterning of the myocardium. *Anat Rec* **258**, 319-337 (2000).
96 Jensen, B. *et al.* The hypertrabeculated (noncompacted) left ventricle is different from the ventricle of embryos and ectothermic vertebrates. *Biochim Biophys Acta* **1863**, 1696-1706, doi:10.1016/j.bbamcr.2015.10.018 (2016).
97 Chen, F. *et al.* Atrioventricular conduction and arrhythmias at the initiation of beating in embryonic mouse hearts. *Dev Dyn* **239**, 1941-1949, doi:10.1002/dvdy.22319 (2010).
98 Rentschler, S. *et al.* Visualization and functional characterization of the developing murine cardiac conduction system. *Development* **128**, 1785-1792 (2001).
99 Valderrabano, M. *et al.* Atrioventricular ring reentry in embryonic mouse hearts. *Circulation* **114**, 543-549, doi:10.1161/CIRCULATIONAHA.106.633727 (2006).
100 Manner, J., Wessel, A. & Yelbuz, T. M. How does the tubular embryonic heart work? Looking for the physical mechanism generating unidirectional blood flow in the valveless embryonic heart tube. *Dev Dyn* **239**, 1035-1046, doi:10.1002/dvdy.22265 (2010).
101 Makikallio, K., Jouppila, P. & Rasanen, J. Human fetal cardiac function during the first trimester of pregnancy. *Heart* **91**, 334-338, doi:10.1136/hrt.2003.029736 (2005).
102 Santhanakrishnan, A., Nguyen, N., Cox, J. G. & Miller, L. A. Flow within models of the vertebrate embryonic heart. *J Theor Biol* **259**, 449-461, doi:10.1016/j.jtbi.2009.04.020 (2009).
103 Hu, N. & Clark, E. B. Hemodynamics of the stage 12 to stage 29 chick embryo. *Circ Res* **65**, 1665-1670 (1989).
104 Wloch, A. *et al.* Doppler study of the embryonic heart in normal pregnant women. *J Matern Fetal Neonatal Med* **20**, 533-539, doi:10.1080/14767050701434747 (2007).
105 Midgett, M., Chivukula, V. K., Dorn, C., Wallace, S. & Rugonyi, S. Blood flow through the embryonic heart outflow tract during cardiac looping in HH13-HH18 chicken embryos. *J R Soc Interface* **12**, 20150652, doi:10.1098/rsif.2015.0652 (2015).
106 Oostra, R. J., Steding, G., Lamers, W. H. & Moorman, A. F. M. *Steding's and Virágh's scanning electron microscopy atlas of the developing human heart*. (Springer, 2007).
107 Wessels, A. *et al.* Spatial distribution of "tissue-specific" antigens in the developing human heart and skeletal muscle. I. An immunohistochemical analysis of creatine kinase isoenzyme expression patterns. *Anat Rec* **228**, 163-176, doi:10.1002/ar.1092280208 (1990).

108 Lamers, W. H. & Moorman, A. F. Cardiac septation: a late contribution of the embryonic primary myocardium to heart morphogenesis. *Circ Res* **91**, 93-103 (2002).

109 Graham, A., Poopalasundaram, S., Shone, V. & Kiecker, C. A reappraisal and revision of the numbering of the pharyngeal arches. *J Anat* **235**, 1019-1023, doi:10.1111/joa.13067 (2019).

110 Fukiishi, Y. & Morriss-Kay, G. M. Migration of cranial neural crest cells to the pharyngeal arches and heart in rat embryos. *Cell Tissue Res* **268**, 1-8, doi:10.1007/BF00338048 (1992).

111 van den Berg, G. *et al.* A caudal proliferating growth center contributes to both poles of the forming heart tube. *Circ Res* **104**, 179-188, doi:10.1161/CIRCRESAHA.108.185843 (2009).

112 Jiang, X., Rowitch, D. H., Soriano, P., McMahon, A. P. & Sucov, H. M. Fate of the mammalian cardiac neural crest. *Development* **127**, 1607-1616 (2000).

113 Phillips, H. M. *et al.* Neural crest cells are required for correct positioning of the developing outflow cushions and pattern the arterial valve leaflets. *Cardiovasc Res* **99**, 452-460, doi:10.1093/cvr/cvt132 (2013).

114 Lincoln, J., Alfieri, C. M. & Yutzey, K. E. Development of heart valve leaflets and supporting apparatus in chicken and mouse embryos. *Dev Dyn* **230**, 239-250, doi:10.1002/dvdy.20051 (2004).

115 Jin, H. *et al.* Differential contribution of the two waves of cardiac progenitors and their derivatives to aorta and pulmonary artery. *Dev Biol* **450**, 82-89, doi:10.1016/j.ydbio.2019.03.019 (2019).

116 Li, D., Angermeier, A. & Wang, J. Planar cell polarity signaling regulates polarized second heart field morphogenesis to promote both arterial and venous pole septation. *Development* **146**, doi:10.1242/dev.181719 (2019).

117 Liang, S. *et al.* Pulmonary endoderm, second heart field and the morphogenesis of distal outflow tract in mouse embryonic heart. *Dev Growth Differ* **56**, 276-292, doi:10.1111/dgd.12129 (2014).

118 Zhou, Z. *et al.* Temporally distinct Six2-positive second heart field progenitors regulate mammalian heart development and disease. *Cell Rep* **18**, 1019-1032, doi:10.1016/j.celrep.2017.01.002 (2017).

119 Ramsbottom, S. A. *et al.* Vangl2-regulated polarisation of second heart field-derived cells is required for outflow tract lengthening during cardiac development. *PLoS Genet* **10**, e1004871, doi:10.1371/journal.pgen.1004871 (2014).

120 Francou, A., De Bono, C. & Kelly, R. G. Epithelial tension in the second heart field promotes mouse heart tube elongation. *Nat Commun* **8**, 14770, doi:10.1038/ncomms14770 (2017).

121 Tada, M. & Heisenberg, C. P. Convergent extension: using collective cell migration and cell intercalation to shape embryos. *Development* **139**, 3897-3904, doi:10.1242/dev.073007 (2012).

122 Sizarov, A. *et al.* Three-dimensional and molecular analysis of the arterial pole of the developing human heart. *J Anat* **220**, 336-349, doi:10.1111/j.1469-7580.2012.01474.x (2012).

123 Eley, L. *et al.* A novel source of arterial valve cells linked to bicuspid aortic valve without raphe in mice. *Elife* **7**, doi:10.7554/eLife.34110 (2018).

124 Tandler, J. in *Manual of human embryology* Vol. II (eds F. Keibel & F. P. Mall) Ch. XVIII, 534-570 (J. B. Lippincott Co, 1912).

125 Okamoto, N., Akimoto, N., Satow, Y., Hidaka, N. & Miyabara, S. *Role of cell death on conal ridges of developing human heart*. Vol. 5 127-137 (Raven Press, 1981).

126 Phillips, H. M., Murdoch, J. N., Chaudhry, B., Copp, A. J. & Henderson, D. J. Vangl2 acts via RhoA signaling to regulate polarized cell movements during development of the proximal outflow tract. *Circ Res* **96**, 292-299, doi:10.1161/01.RES.0000154912.08695.88 (2005).

127 Anderson, R. H., Spicer, D. E., Mohun, T. J., Hikspoors, J. & Lamers, W. H. Remodeling of the embryonic interventricular communication in regard to the description and classification of ventricular septal defects. *Anat Rec (Hoboken)* **302**, 19-31, doi:10.1002/ar.24020 (2019).

128 Mall, F. P. On the development of the human heart. *Am J Anat* **13**, 249-298 (1912).

129 Congdon, E. D. Transformation of the aortic-arch system during the development of the human embryo. . *Contrib Embryol, Carnegie Inst Wash* **14**, 47-110 (1922).

130 Yang, Y. P., Li, H. R., Cao, X. M., Qiao, C. J. & Ya, J. Septation of the intrapericardial arterial trunks in the early human embryonic heart. *Chin Med J (Engl)* **131**, 1457-1464, doi:10.4103/0366-6999.233956 (2018).

131 Sawada, H., Rateri, D. L., Moorleghen, J. J., Majesky, M. W. & Daugherty, A. Smooth muscle cells derived from second heart field and cardiac neural crest reside in spatially distinct domains in the media of the ascending aorta-brief report. *Arterioscler Thromb Vasc Biol* **37**, 1722-1726, doi:10.1161/ATVBAHA.117.309599 (2017).
132 Rana, M. S., Sizarov, A., Christoffels, V. M. & Moorman, A. F. Development of the human aortic arch system captured in an interactive three-dimensional reference model. *Am J Med Genet A* **164A**, 1372-1383, doi:10.1002/ajmg.a.35881 (2014).
133 Anderson, R. H., Brown, N. A. & Webb, S. Development and structure of the atrial septum. *Heart* **88**, 104-110 (2002).
134 Snarr, B. S. *et al.* Isl1 expression at the venous pole identifies a novel role for the second heart field in cardiac development. *Circ Res* **101**, 971-974, doi:10.1161/CIRCRESAHA.107.162206 (2007).
135 Lamers, W. H., Viragh, S., Wessels, A., Moorman, A. F. & Anderson, R. H. Formation of the tricuspid valve in the human heart. *Circulation* **91**, 111-121 (1995).
136 Vassall-Adams, P. R. The development of the atrioventricular bundle and its branches in the avian heart. *J Anat* **134**, 169-183 (1982).
137 Bajolle, F. *et al.* Myocardium at the base of the aorta and pulmonary trunk is prefigured in the outflow tract of the heart and in subdomains of the second heart field. *Dev Biol* **313**, 25-34, doi:10.1016/j.ydbio.2007.09.023 (2008).
138 Yashiro, K., Shiratori, H. & Hamada, H. Haemodynamics determined by a genetic programme govern asymmetric development of the aortic arch. *Nature* **450**, 285-288, doi:10.1038/nature06254 (2007).
139 Phoon, C. K., Aristizabal, O. & Turnbull, D. H. 40 MHz Doppler characterization of umbilical and dorsal aortic blood flow in the early mouse embryo. *Ultrasound Med Biol* **26**, 1275-1283, doi:10.1016/s0301-5629(00)00278-7 (2000).
140 Kaba, R. A. *et al.* Comparison of connexin 43, 40 and 45 expression patterns in the developing human and mouse hearts. *Cell Commun Adhes* **8**, 339-343 (2001).
141 Van Kempen, M. J. *et al.* Developmental changes of connexin40 and connexin43 mRNA distribution patterns in the rat heart. *Cardiovasc Res* **32**, 886-900 (1996).
142 Wenink, A. C., Knaapen, M. W., Vrolijk, B. C. & VanGroningen, J. P. Development of myocardial fiber organization in the rat heart. *Anat Embryol (Berl)* **193**, 559-567 (1996).
143 Samsa, L. A., Yang, B. & Liu, J. Embryonic cardiac chamber maturation: Trabeculation, conduction, and cardiomyocyte proliferation. *Am J Med Genet C Semin Med Genet* **163C**, 157-168, doi:10.1002/ajmg.c.31366 (2013).
144 Sedmera, D. & McQuinn, T. Embryogenesis of the heart muscle. *Heart Fail Clin* **4**, 235-245, doi:10.1016/j.hfc.2008.02.007 (2008).
145 Jensen, B., van der Wal, A. C., Moorman, A. F. M. & Christoffels, V. M. Excessive trabeculations in noncompaction do not have the embryonic identity. *Int J Cardiol* **227**, 325-330, doi:10.1016/j.ijcard.2016.11.089 (2017).
146 Knaapen, M. W., Vrolijk, B. C. & Wenink, A. C. Growth of the myocardial volumes of the individual cardiac segments in the rat embryo. *Anat Rec* **243**, 93-100, doi:10.1002/ar.1092430111 (1995).
147 Goor, D. A., Dische, R. & Lillehei, C. W. The conotruncus. I. Its normal inversion and conus absorption. *Circulation* **46**, 375-384, doi:10.1161/01.cir.46.2.375 (1972).
148 van den Hoff, M. J. *et al.* Myocardialization of the cardiac outflow tract. *Dev Biol* **212**, 477-490, doi:10.1006/dbio.1999.9366 (1999).
149 Padget, D. H. Designation of the embryonic intersegmental arteries in reference to the vertebral artery and subclavian stem. *Anat Rec* **119**, 349-356, doi:10.1002/ar.1091190306 (1954).
150 Harmon, A. W. & Nakano, A. Nkx2-5 lineage tracing visualizes the distribution of second heart field-derived aortic smooth muscle. *Genesis* **51**, 862-869, doi:10.1002/dvg.22721 (2013).
151 Verzi, M. P., McCulley, D. J., De Val, S., Dodou, E. & Black, B. L. The right ventricle, outflow tract, and ventricular septum comprise a restricted expression domain within the secondary/anterior heart field. *Dev Biol* **287**, 134-145, doi:10.1016/j.ydbio.2005.08.041 (2005).
152 Gittenberger-de Groot, A. C. *et al.* The arterial and cardiac epicardium in development, disease and repair. *Differentiation* **84**, 41-53, doi:10.1016/j.diff.2012.05.002 (2012).

153 Manner, J. Does the subepicardial mesenchyme contribute myocardioblasts to the myocardium of the chick embryo heart? A quail-chick chimera study tracing the fate of the epicardial primordium. *Anat Rec* **255**, 212-226, doi:10.1002/(sici)1097-0185(19990601)255:2<212::aid-ar11>3.3.co;2-o (1999).
154 Perez-Pomares, J. M., Phelps, A., Sedmerova, M. & Wessels, A. Epicardial-like cells on the distal arterial end of the cardiac outflow tract do not derive from the proepicardium but are derivatives of the cephalic pericardium. *Dev Dyn* **227**, 56-68, doi:10.1002/dvdy.10284 (2003).
155 Gittenberger-de Groot, A. C., Vrancken Peeters, M. P., Bergwerff, M., Mentink, M. M. & Poelmann, R. E. Epicardial outgrowth inhibition leads to compensatory mesothelial outflow tract collar and abnormal cardiac septation and coronary formation. *Circ Res* **87**, 969-971, doi:10.1161/01.res.87.11.969 (2000).
156 Odgers, P. N. The development of the pars membranacea septi in the human heart. *J Anat* **72**, 247-259 (1938).
157 Lamers, W. H., De Jong, F., De Groot, I. J. & Moorman, A. F. The development of the avian conduction system, a review. *Eur J Morphol* **29**, 233-253 (1991).
158 Kim, J. S., Viragh, S., Moorman, A. F., Anderson, R. H. & Lamers, W. H. Development of the myocardium of the atrioventricular canal and the vestibular spine in the human heart. *Circ Res* **88**, 395-402, doi:10.1161/01.res.88.4.395 (2001).
159 Zhao, Z. & Rivkees, S. A. Programmed cell death in the developing heart: regulation by BMP4 and FGF2. *Dev Dyn* **217**, 388-400, doi:10.1002/(SICI)1097-0177(200004)217:4<388::AID-DVDY6>3.0.CO;2-N (2000).
160 Cheng, G., Wessels, A., Gourdie, R. G. & Thompson, R. P. Spatiotemporal and tissue specific distribution of apoptosis in the developing chick heart. *Dev Dyn* **223**, 119-133, doi:10.1002/dvdy.1244 (2002).
161 Sharma, P. R., Anderson, R. H., Copp, A. J. & Henderson, D. J. Spatiotemporal analysis of programmed cell death during mouse cardiac septation. *Anat Rec A Discov Mol Cell Evol Biol* **277**, 355-369, doi:10.1002/ar.a.20006 (2004).
162 Nakamura, T., Colbert, M. C. & Robbins, J. Neural crest cells retain multipotential characteristics in the developing valves and label the cardiac conduction system. *Circ Res* **98**, 1547-1554, doi:10.1161/01.RES.0000227505.19472.69 (2006).
163 Merrick, A. F., Yacoub, M. H., Ho, S. Y. & Anderson, R. H. Anatomy of the muscular subpulmonary infundibulum with regard to the Ross procedure. *Ann Thorac Surg* **69**, 556-561, doi:10.1016/s0003-4975(99)01300-4 (2000).
164 Anderson, R. H. *et al.* Myths and realities relating to development of the arterial valves. *J. Cardiovasc. Dev. Dis.* **1**, 177-200 (2014).
165 Ya, J. *et al.* Normal development of the outflow tract in the rat. *Circ Res* **82**, 464-472 (1998).
166 Steding, G. in *The anatomy of the human embryo; a scanning electron-microscopic atlas* Ch. 3.1, 204-253 (Karger, 2009).
167 Chen, H. I. *et al.* VEGF-C and aortic cardiomyocytes guide coronary artery stem development. *J Clin Invest* **124**, 4899-4914, doi:10.1172/JCI77483 (2014).
168 Theveniau-Ruissy, M. *et al.* Coronary stem development in wild-type and Tbx1 null mouse hearts. *Dev Dyn* **245**, 445-459, doi:10.1002/dvdy.24380 (2016).
169 Bogers, A. J., Gittenberger-de Groot, A. C., Dubbeldam, J. A. & Huysmans, H. A. The inadequacy of existing theories on development of the proximal coronary arteries and their connexions with the arterial trunks. *Int J Cardiol* **20**, 117-123, doi:10.1016/0167-5273(88)90321-x (1988).
170 Conte, G. & Pellegrini, A. On the development of the coronary arteries in human embryos, stages 14-19. *Anat Embryol (Berl)* **169**, 209-218, doi:10.1007/bf00303151 (1984).
171 Hirakow, R. Development of the cardiac blood vessels in staged human embryos. *Acta Anat (Basel)* **115**, 220-230, doi:10.1159/000145693 (1983).
172 Hutchins, G. M., Kessler-Hanna, A. & Moore, G. W. Development of the coronary arteries in the embryonic human heart. *Circulation* **77**, 1250-1257, doi:10.1161/01.cir.77.6.1250 (1988).
173 Tomanek, R. J. Developmental progression of the coronary vasculature in human embryos and fetuses. *Anat Rec (Hoboken)* **299**, 25-41, doi:10.1002/ar.23283 (2016).

174 Kelleher, C. M., McLean, S. E. & Mecham, R. P. Vascular extracellular matrix and aortic development. *Curr Top Dev Biol* **62**, 153-188, doi:10.1016/S0070-2153(04)62006-0 (2004).
175 Streeter, G. L. in *Contrib Embryol,* Vol. 34 (eds C.H. Heuser & G.W. Corner) Ch. 165, 165-196 (Carnegie Inst Wash, 1951).
176 Teal, S. I., Moore, G. W. & Hutchins, G. M. Development of aortic and mitral valve continuity in the human embryonic heart. *Am J Anat* **176**, 447-460, doi:10.1002/aja.1001760407 (1986).
177 Anderson, R. H., Spicer, D. E., Brown, N. A. & Mohun, T. J. The development of septation in the four-chambered heart. *Anat Rec (Hoboken)* **297**, 1414-1429, doi:10.1002/ar.22949 (2014).
178 Allwork, S. P. & Anderson, R. H. Developmental anatomy of the membranous part of the ventricular septum in the human heart. *Br Heart J* **41**, 275-280, doi:10.1136/hrt.41.3.275 (1979).
179 Kim, D. T. *et al.* The ligament of Marshall: a structural analysis in human hearts with implications for atrial arrhythmias. *J Am Coll Cardiol* **36**, 1324-1327, doi:10.1016/s0735-1097(00)00819-6 (2000).
180 Cabrera, J. A., Ho, S. Y., Climent, V. & Sanchez-Quintana, D. The architecture of the left lateral atrial wall: a particular anatomic region with implications for ablation of atrial fibrillation. *Eur Heart J* **29**, 356-362, doi:10.1093/eurheartj/ehm606 (2008).
181 Magovern, J. H., Moore, G. W. & Hutchins, G. M. Development of the atrioventricular valve region in the human embryo. *Anat Rec* **215**, 167-181, doi:10.1002/ar.1092150210 (1986).
182 Wessels, A. *et al.* Epicardially derived fibroblasts preferentially contribute to the parietal leaflets of the atrioventricular valves in the murine heart. *Dev Biol* **366**, 111-124, doi:10.1016/j.ydbio.2012.04.020 (2012).
183 Ebadi, A., Spicer, D. E., Backer, C. L., Fricker, F. J. & Anderson, R. H. Double-outlet right ventricle revisited. *J Thorac Cardiovasc Surg* **154**, 598-604, doi:10.1016/j.jtcvs.2017.03.049 (2017).
184 Jauniaux, E., Hempstock, J., Greenwold, N. & Burton, G. J. Trophoblastic oxidative stress in relation to temporal and regional differences in maternal placental blood flow in normal and abnormal early pregnancies. *Am J Pathol* **162**, 115-125, doi:10.1016/S0002-9440(10)63803-5 (2003).
185 O'Rahilly, R. & Muller, F. Somites, spinal ganglia, and centra. Enumeration and interrelationships in staged human embryos, and implications for neural tube defects. *Cells Tissues Organs* **173**, 75-92, doi:10.1159/000068948 (2003).
186 Theiler, K. *The house mouse. Development and normal stages from fertilization to 4 weeks of age.*, (Springer-Verlag, 1972).
187 Runciman, S. I., Gannon, B. J. & Baudinette, R. V. Central cardiovascular shunts in the perinatal marsupial. *Anat Rec* **243**, 71-83, doi:10.1002/ar.1092430109 (1995).
188 Kaufman, M. H. & Navaratnam, V. Early differentiation of the heart in mouse embryos. *J Anat* **133**, 235-246 (1981).
189 Wessels, A. *et al.* Spatial distribution of "tissue-specific" antigens in the developing human heart and skeletal muscle. II. An immunohistochemical analysis of myosin heavy chain isoform expression patterns in the embryonic heart. *Anat Rec* **229**, 355-368, doi:10.1002/ar.1092290309 (1991).
190 Sizarov, A. *et al.* Molecular analysis of patterning of conduction tissues in the developing human heart. *Circ Arrhythm Electrophysiol* **4**, 532-542, doi:10.1161/CIRCEP.111.963421 (2011).
191 Kirby, M. L. *Cardiac development*. (Oxford University Press, 2007).
192 Hamburger, V. & Hamilton, H. L. A series of normal stages in the development of the chick embryo. *J Morphol* **88**, 49-92 (1951).
193 Martinsen, B. J. Reference guide to the stages of chick heart embryology. *Dev Dyn* **233**, 1217-1237, doi:10.1002/dvdy.20468 (2005).
194 Anderson, R. H. *et al.* Sequential segmental analysis of congenital heart disease. *Pediatr Cardiol* **5**, 281-287, doi:10.1007/BF02424973 (1984).

Figures

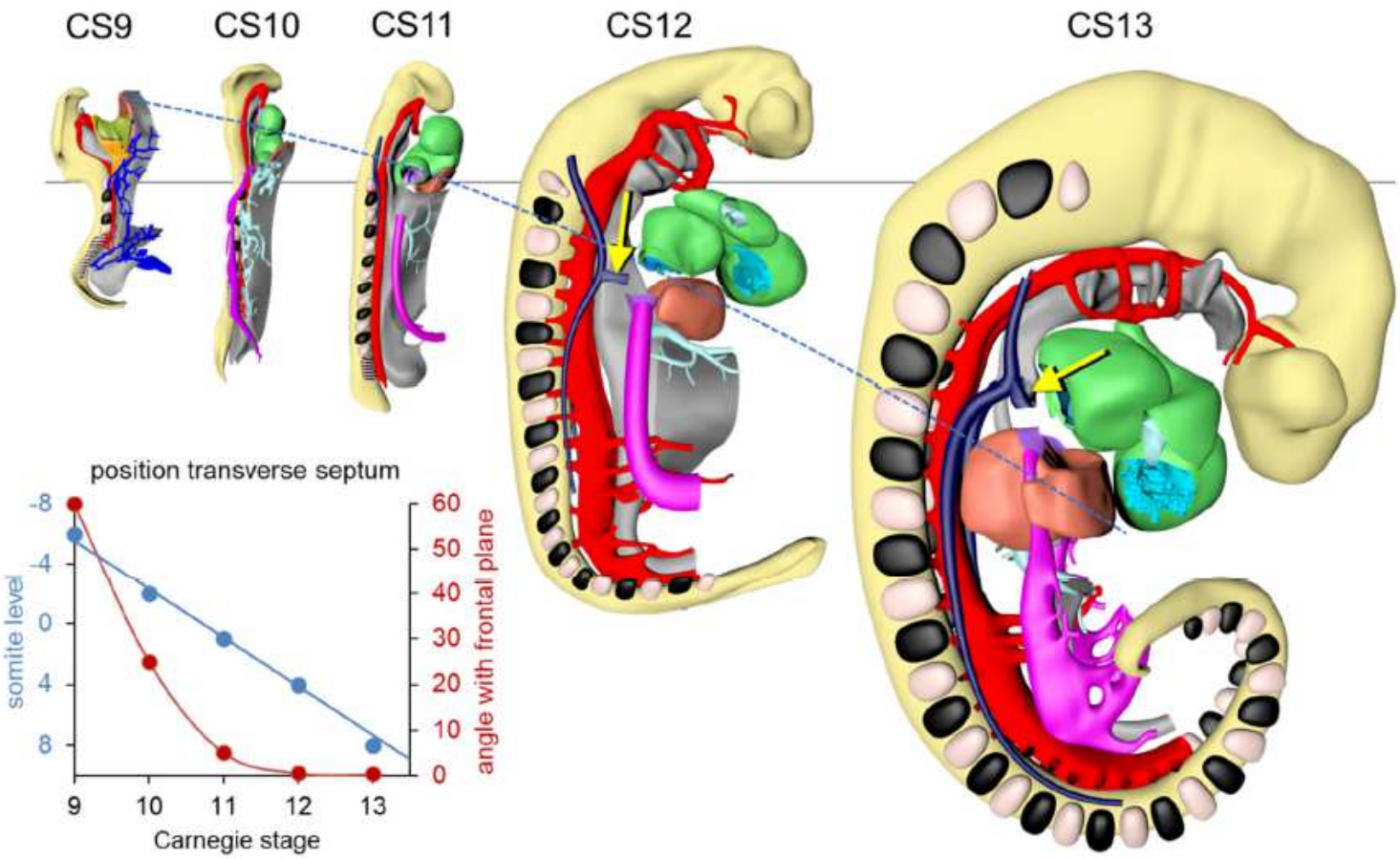

Figure 1

Pictorial timeline of the ‘descent” of the transverse septum.

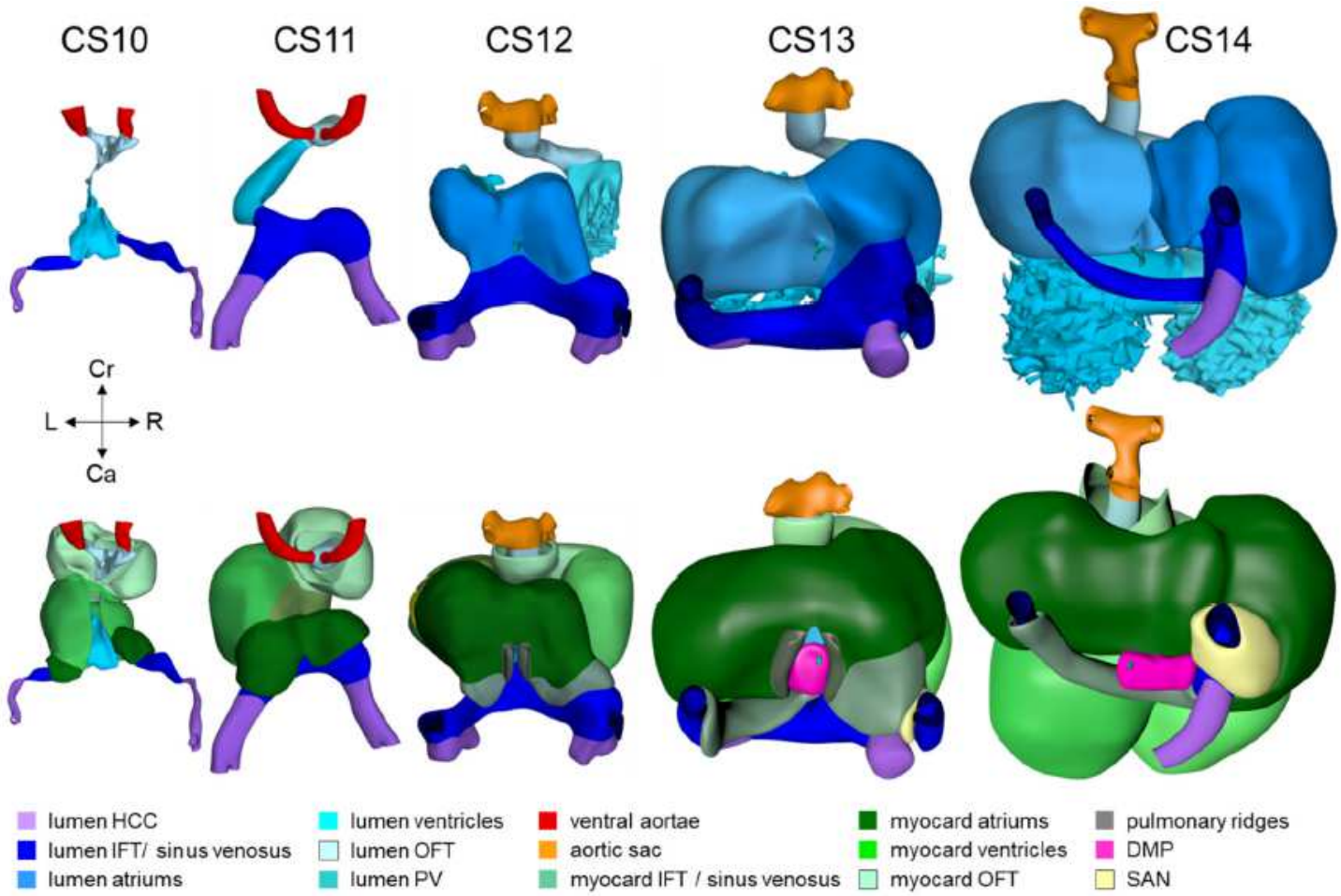

Figure 2

Pictorial timeline of the development of the inflow tract.

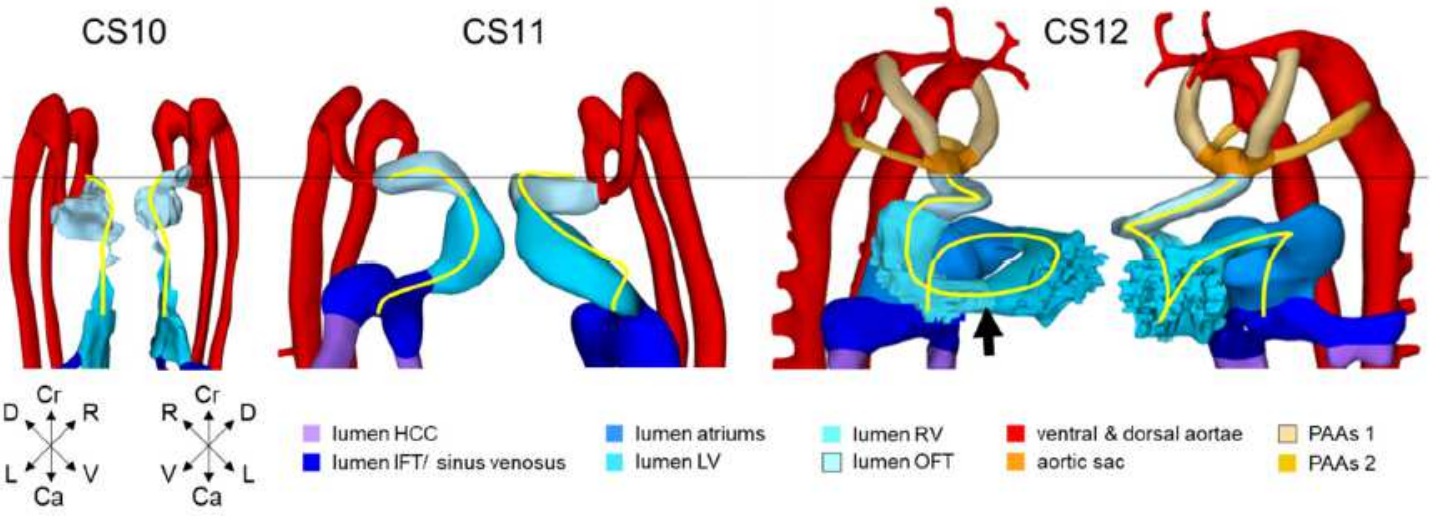

Figure 3

Looping of the heart tube.

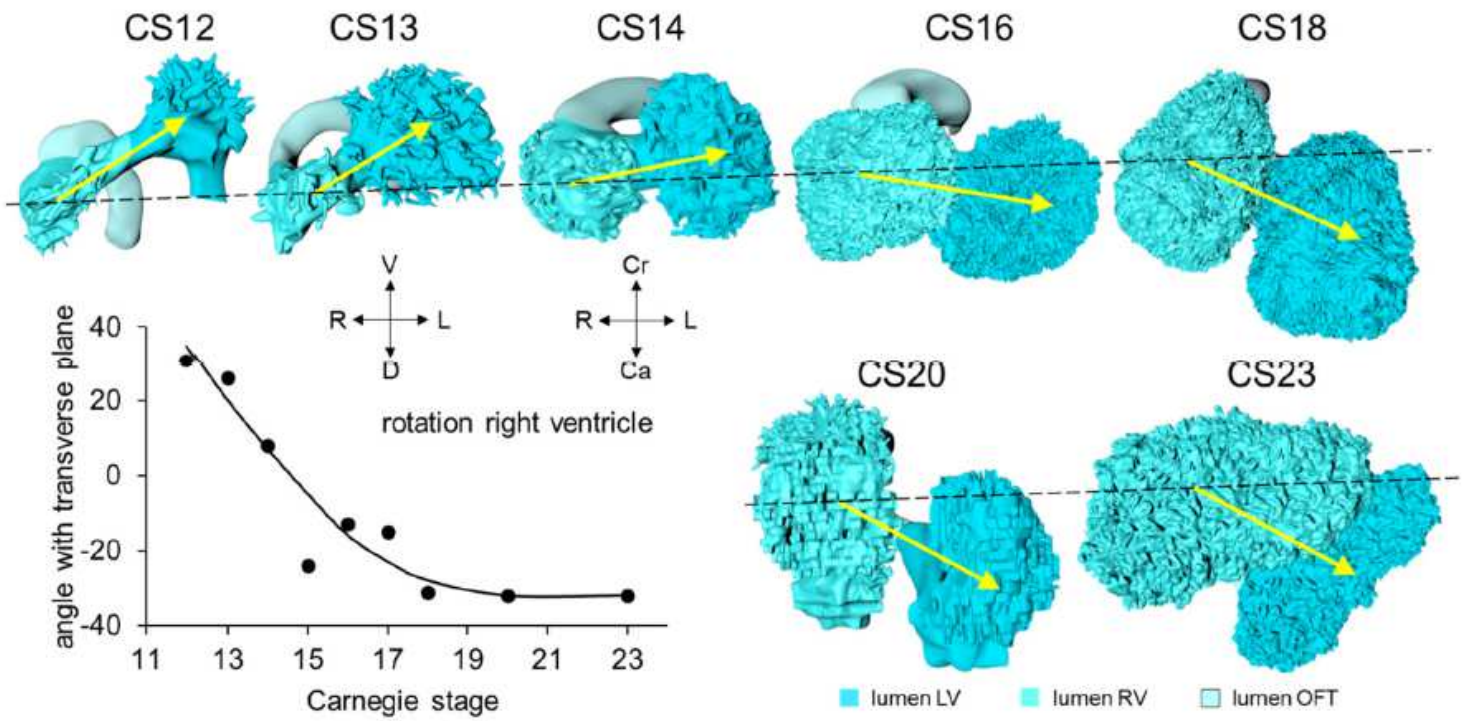

Figure 4

Pictorial timeline of the changing position of the developing right ventricle.

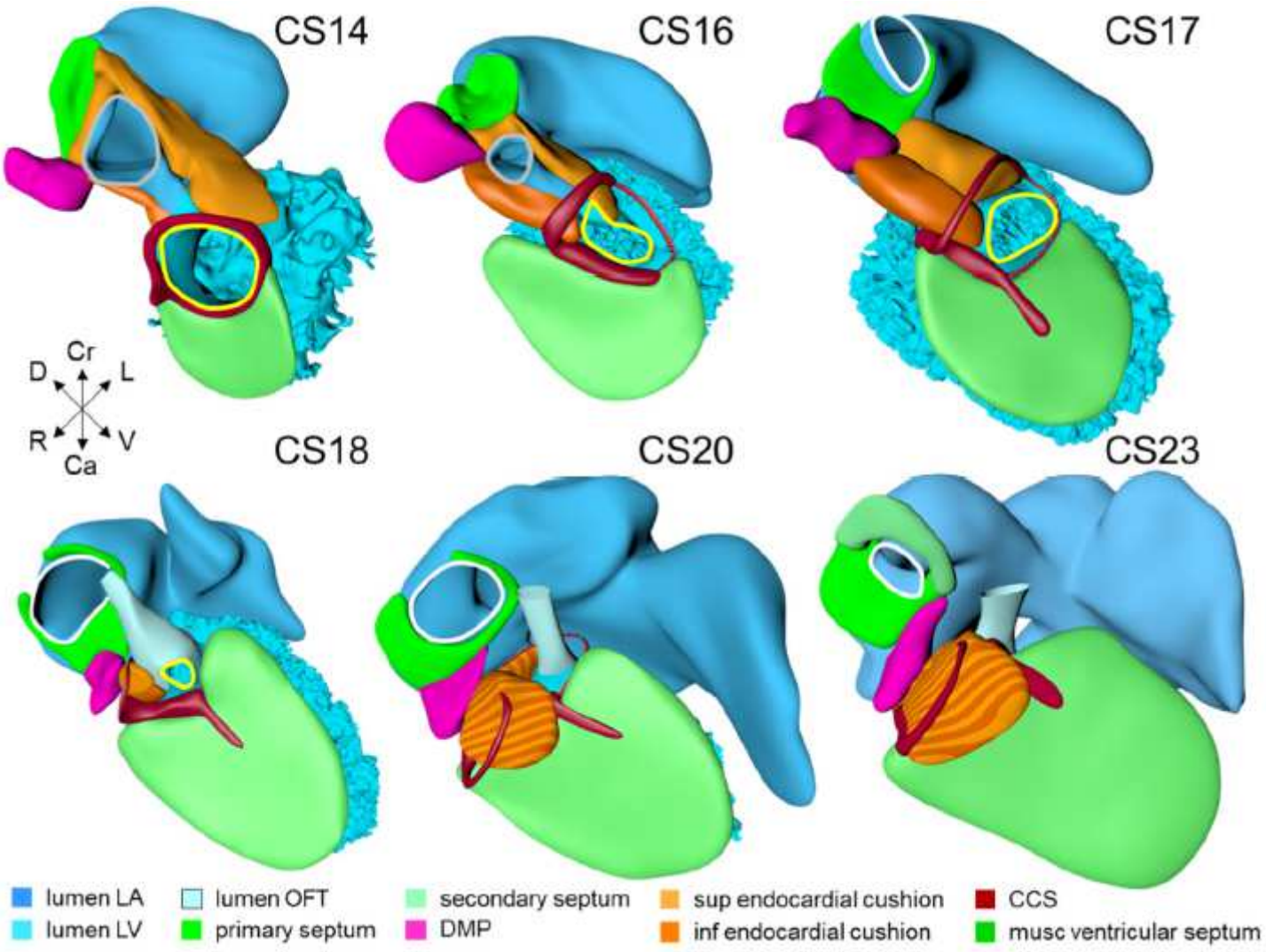

Figure 5

Pictorial timeline of the closure of the interatrial & interventricular foramens.

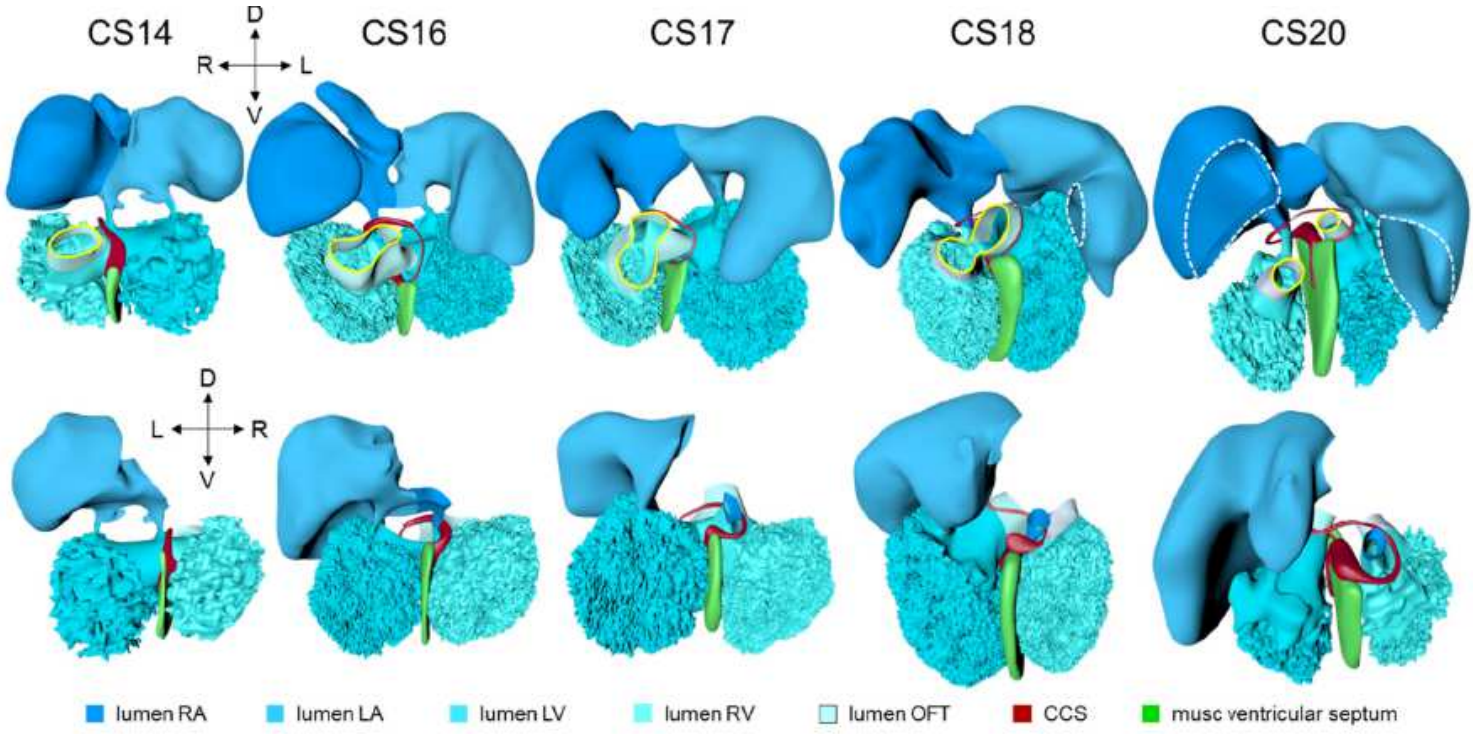

Figure 6

Pictorial timeline of the subdivision of the interventricular foramen into the peri tricuspid inlet, subaortic outlet, and membranous septum.

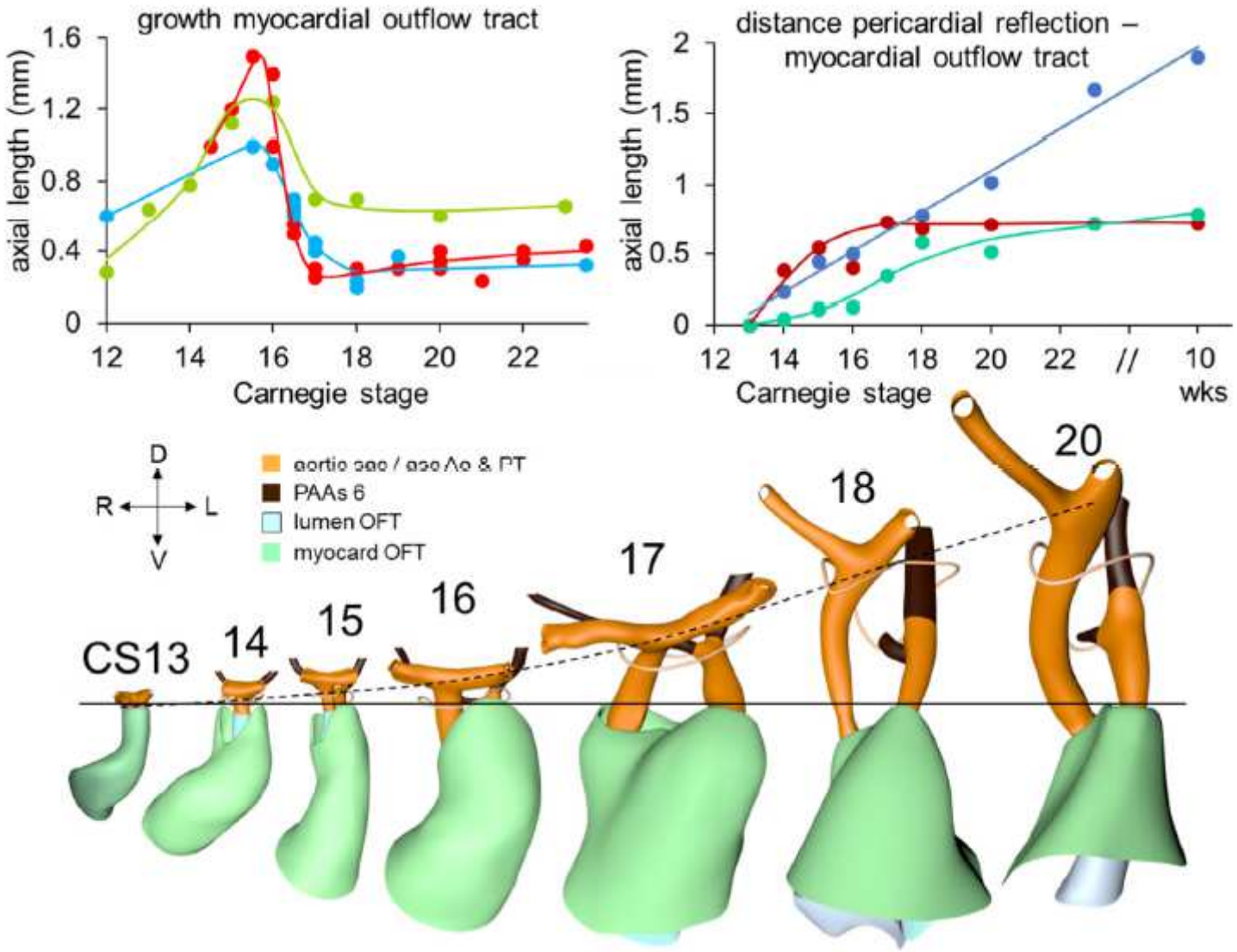

Figure 7

Changes in size and shape of the myocardial outflow tract and arterial trunks.

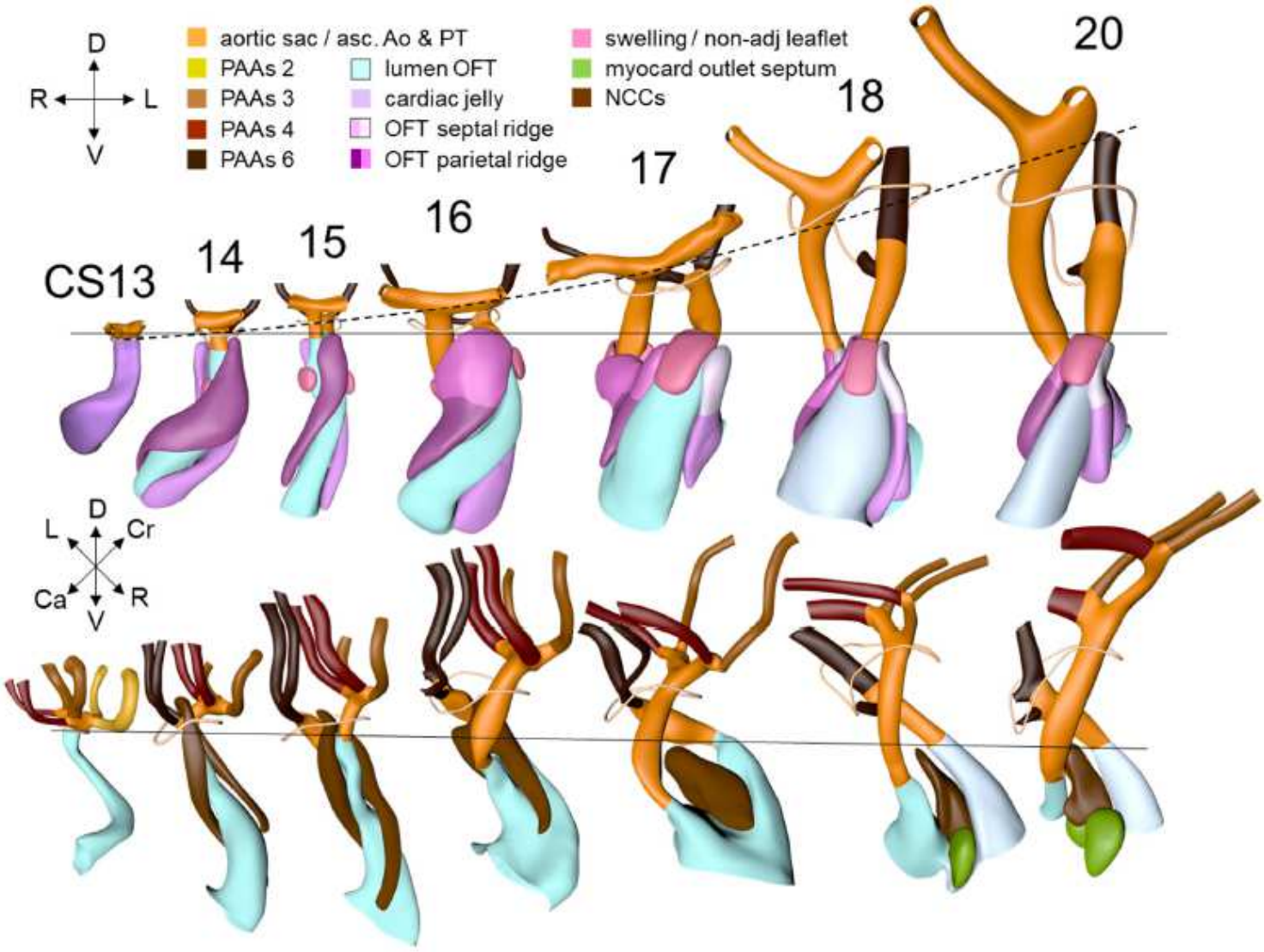

Figure 8

Pictorial timeline of the changes in size and shape of the lumen, endocardial ridges and swellings, and neural-crest prongs of the outflow tract.

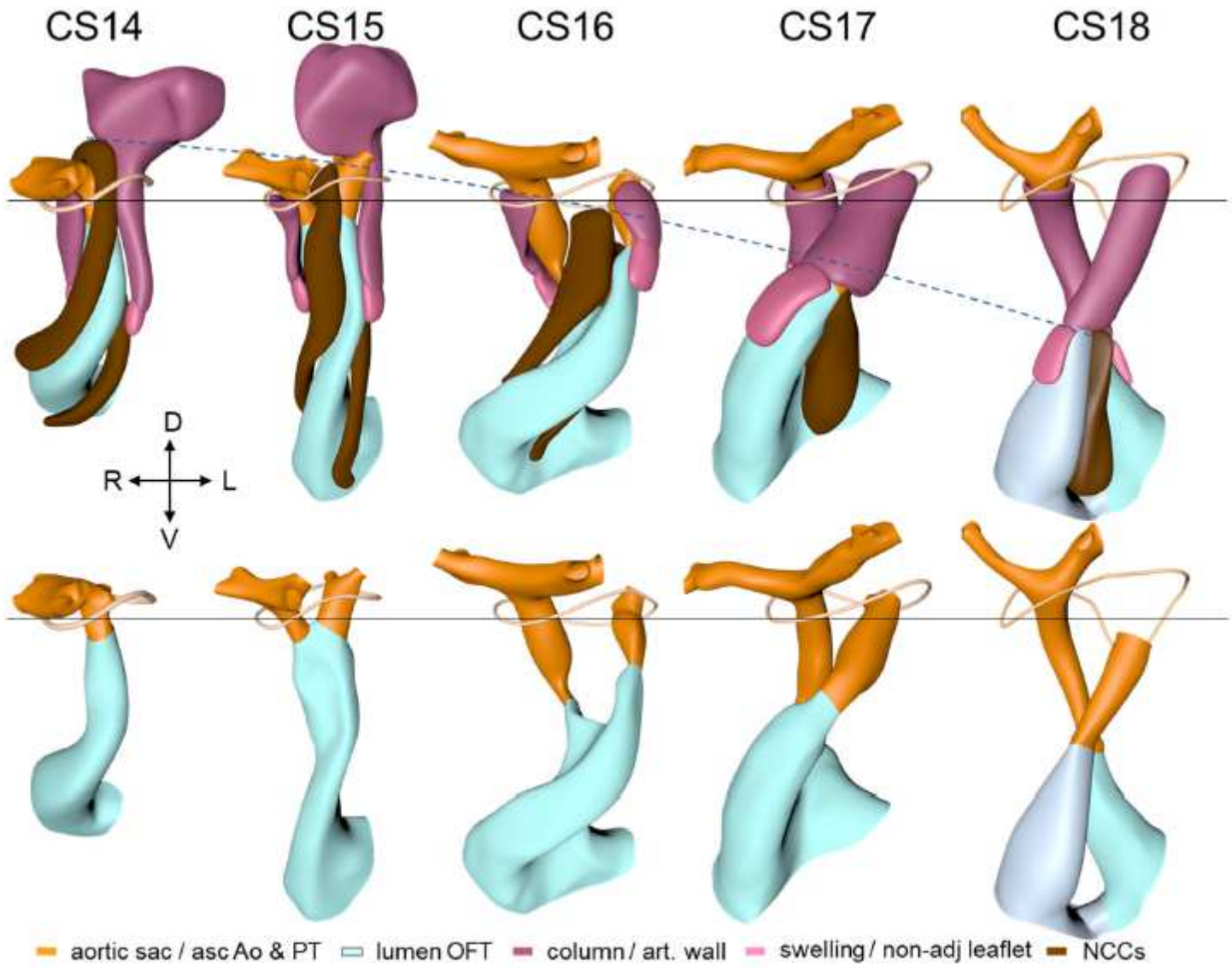

Figure 9

Pictorial timeline of the appearance of the non-myocardial walls of the arterial trunks.

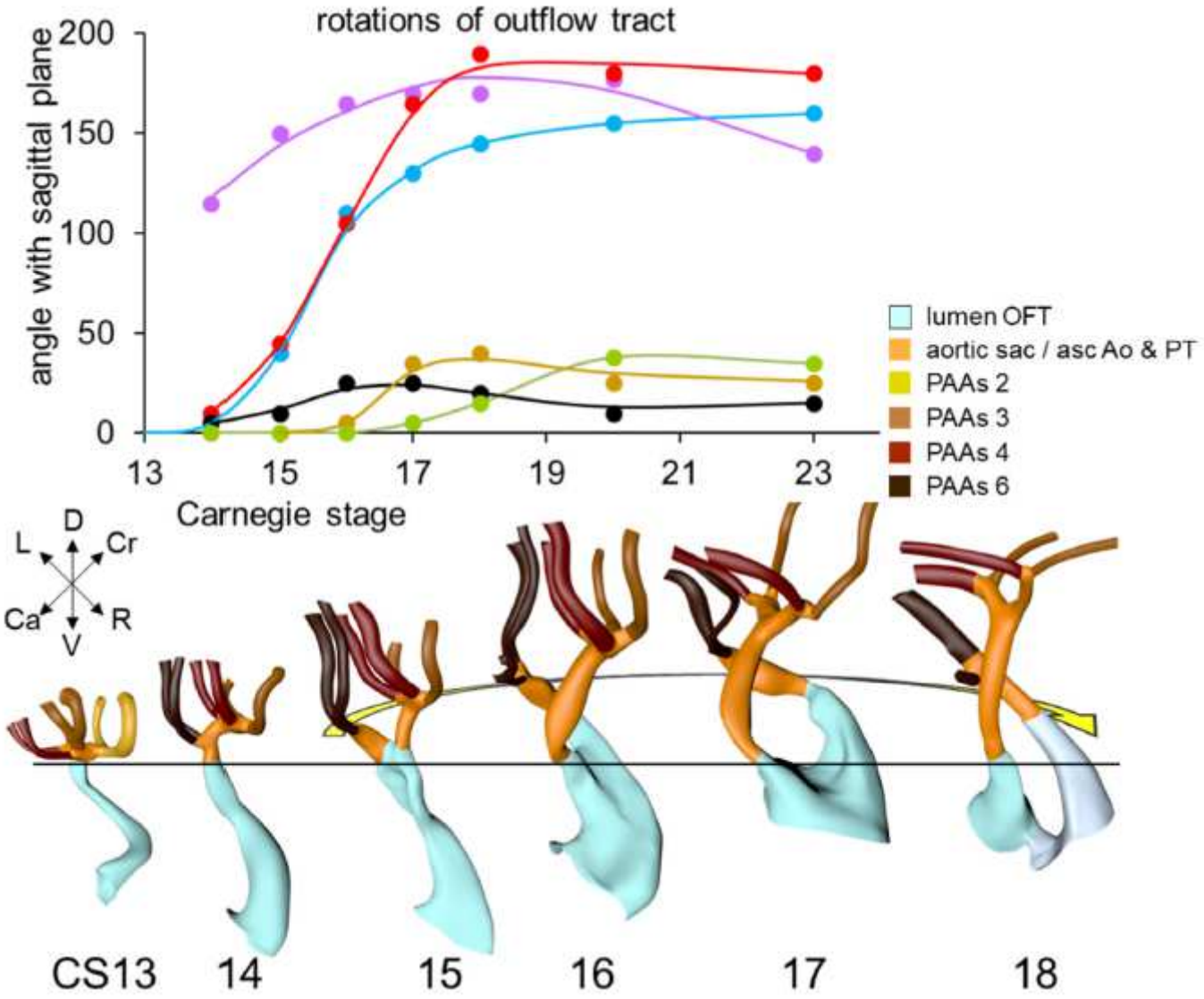

Figure 10

Changes in the course of the (sub-)aortic and (sub-)pulmonary channels.

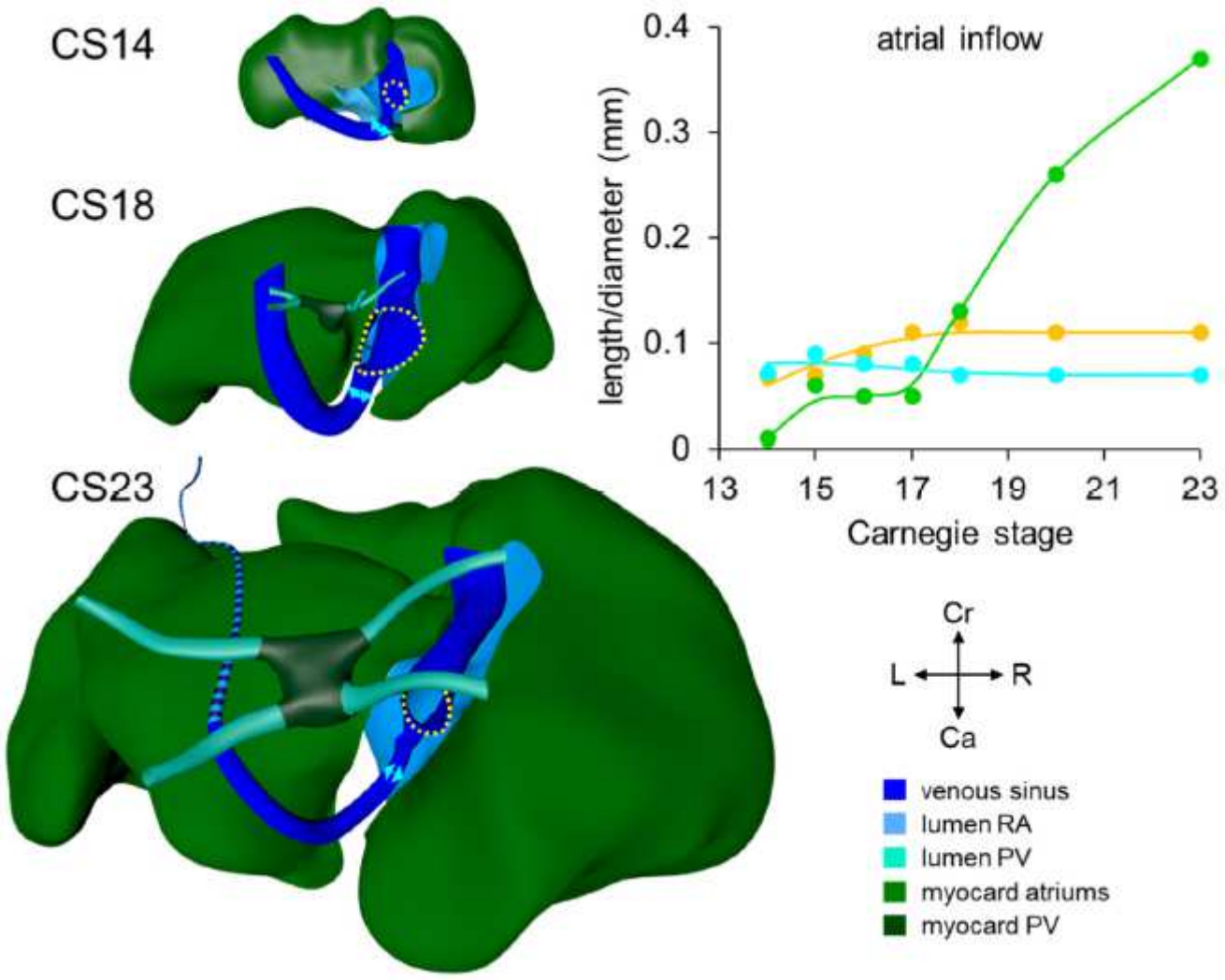

Figure 11

Pictorial timeline of the developing pulmonary veins and coronary sinus.

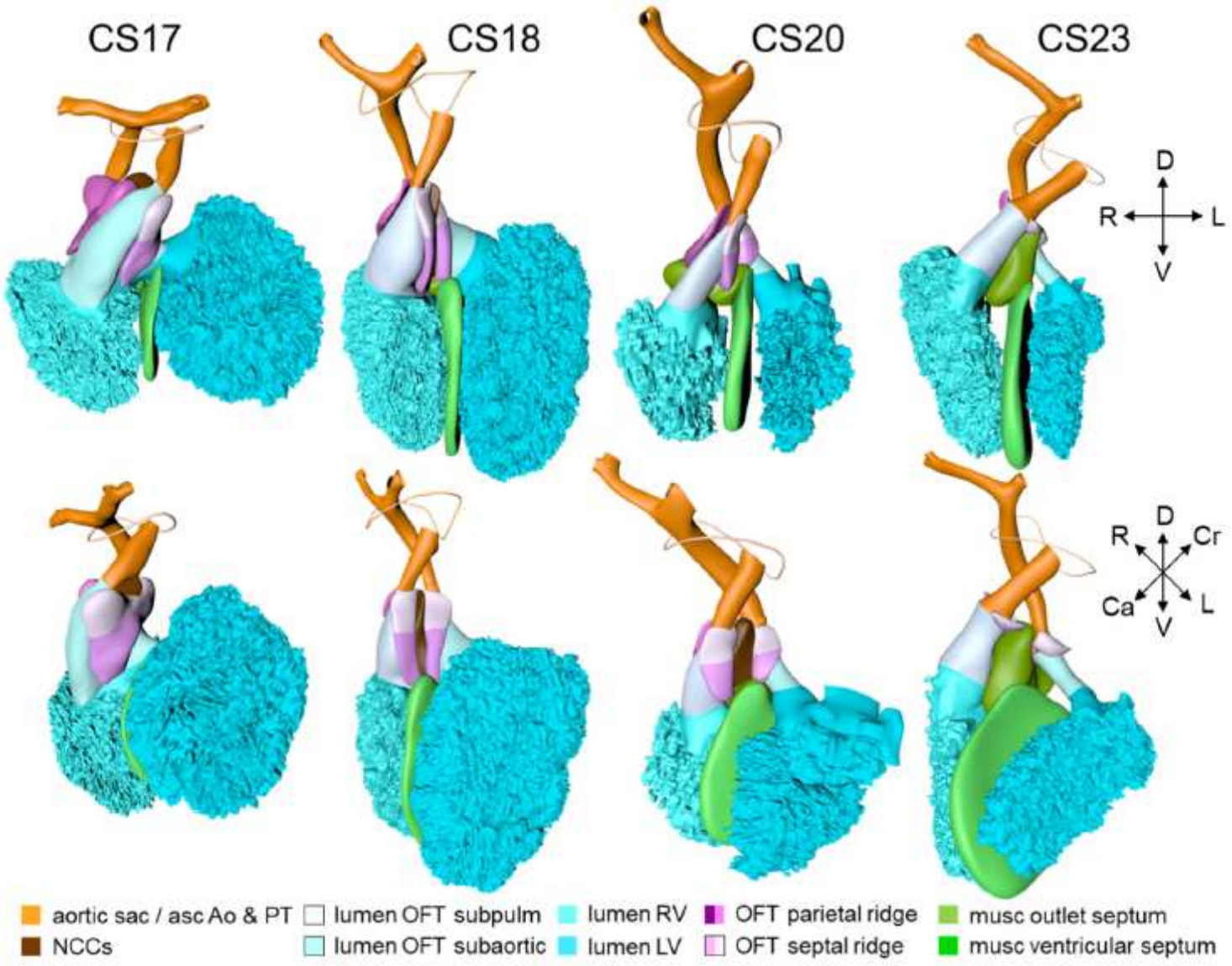

Figure 12

Pictorial timeline of the formation of the subpulmonary infundibulum.

Supplementary Files

This is a list of supplementary files associated with this preprint. Click to download.

- SupplementalTablesXFiguresHikspoors.pdf